Quaternary Science Reviews 135 (2016) 1–23

Contents lists available at ScienceDirect

Quaternary Science Reviews

journal homepage: www.elsevier.com/locate/quascirev

Invited review

150,000 years of loess accumulation in central Alaska

Britta J.L. Jensen [a, *, 1], Michael E. Evans [b], Duane G. Froese [a], Vadim A. Kravchinsky [b]

[a] Department of Earth and Atmospheric Sciences, University of Alberta, Edmonton, AB, Canada
[b] Department of Physics, University of Alberta, Edmonton, AB, Canada

ARTICLE INFO

Article history:
Received 1 September 2015
Received in revised form
1 December 2015
Accepted 2 January 2016
Available online 14 January 2016

Keywords:
Loess
Halfway House
Quaternary
Paleosols
Tephra
Magnetic susceptibility
Alaska
Paleomagnetism
Marine isotope stage 5

ABSTRACT

The Halfway House site in interior Alaska is arguably the most studied loess deposit in northwestern North America. The site contains a complex paleomagnetic and paleoenvironmental record, but has lacked the robust chronologic control that would allow its full potential to be exploited. Detailed reexamination of stratigraphy, paleomagnetics and tephrostratigraphy reveals a relatively complete marine isotope stage (MIS) 6 to Holocene record constrained by the Old Crow (124 ± 10 ka), VT (106 ± 10 ka), Sheep Creek-Klondike (ca. 80 ka), Dominion Creek (77 ± 8 ka) and Dawson (ca. 30.2 cal ka BP) tephras. We show two well-developed paleosols formed during Marine Isotope Stages (MIS) 5e and 5a, while MIS 5c and 5b are either poorly represented or absent. The new tephrostratigraphy presented here is the most complete one to date for the late Pleistocene and indicates MIS 5 sediments are more common than previously recognized. A magnetic excursion within the sediments is identified as the post-Blake excursion (94.1 ± 7.8 ka), providing independent age control and adding to the increasing body of evidence that Alaskan loess is a detailed recorder of variations of the Earth's magnetic field over time. A high-resolution magnetic susceptibility profile placed into this new chronostratigraphic framework supports the hypothesis that wind-intensity is the main variable controlling fluctuations in susceptibility. Correlation of the susceptibility record to global marine $\delta^{18}O$ records is complicated by highly variable accumulation rates. We find the lowest rates of accumulation during peak warm and cold stages, while abrupt increases are associated with periods of transition between marine isotope (sub)stages. Building on previous accumulation models for Alaska, surface roughness is likely a leading variable controlling loess accumulation rates during transitions and peak cold periods, but the negligible accumulation during MIS 5e and 5a suggests that loess production was exceedingly low, negating the role of surface roughness. This interplay of variables leads to optimal conditions for loess accumulation during transitions between isotope stages, and to a somewhat lesser extent, stadials and interstadials.

1. Introduction

Large areas of Yukon and Alaska remained unglaciated during the Quaternary, but the proximity to major ice sheets has provided the conditions to create and preserve a loess record spanning more than 3 million years (e.g. Westgate et al., 1990). In this region, commonly known as eastern Beringia, loess deposits are often roughly divided into two main types: valley-bottom and upland loess. Valley-bottom loess is commonly perennially frozen and may be interbedded with retransported loess and organic material related to the growth of syngenetic permafrost and periods of degradation. Sediments are organic-rich, and alluvial and colluvial material may be locally present. These valley-bottom deposits tend to preserve the rich floral and faunal records for which Beringia is famous (e.g. Froese et al., 2006, 2009; Guthrie, 1968, 1990; Péwé, 1975a; Péwé et al., 1997, 2009; Zazula et al., 2007). Upland loess is generally comprised of primary air-fall loess that was, or is, perennially frozen, but has been relatively ice-poor for most of its existence. Most primary deposits have experienced periods where permafrost may have completely thawed (e.g. Péwé, 1975a,b; Péwé et al., 1997), and these fluctuations have caused some reworking and erosion through thaw slumping and cryoturbation. Regardless, this 'upland' loess is more comparable to 'classic' loess deposits, such as the Chinese loess plateau, where dry, organic-poor loess contains numerous paleosols (e.g. Liu et al., 1986; Kukla, 1987; Begét and Hawkins, 1989; Begét, 2001; Muhs et al., 2003, 2008; Jensen et al., 2008). Modern loess deposition is limited, but does

* Corresponding author.
E-mail address: bjjensen@ualberta.ca (B.J.L. Jensen).
[1] Current address: Royal Alberta Museum, Edmonton, AB, Canada.

http://dx.doi.org/10.1016/j.quascirev.2016.01.001
0277-3791/

continue in parts of Alaska, with estimated deposition rates at 0.2–2 mm/year in the Fairbanks area (Pewe, 1955, 1975a).

These extensive deposits, originally referred to as the "Yukon silts," have been mapped since the late 1800s (e.g. Russell, 1890; Spurr and Goodrich, 1898; Gilmore, 1908). The origins of the silt were unclear, with most workers suggesting a number of different processes, although by the 1950s, Taber's (1943, 1953) hypothesis of *in situ* production by frost-shattering was in vogue. However, subsequent detailed work by his contemporary Troy Péwé (1955) presented a compelling argument that the silts were aeolian deposits. Péwé (1955) noted that these silts were thickest along or near the major silt-rich and glacially-fed rivers of Alaska, and tended to thin away from them, both laterally and with elevation. Most importantly, he also noted that the mineralogy of the loess differed from the underlying bedrock, effectively disproving Taber's *in situ* hypothesis. This alternative hypothesis was not without controversy but was largely accepted not long after it was first presented.

Péwé went on to formalize the stratigraphic nomenclature for these silts in the Fairbanks region (Péwé, 1975b). Valley-bottom retransported loess was thought to be primarily post-last interglacial (i.e. marine isotope stage (MIS) 5) in age, and was divided into the Wisconsinan Goldstream Formation (MIS 4–2) and Holocene Ready Bullion (MIS 1) Formation. Primary loess deposits, which tend to mantle mid-slope and upland portions of central Alaska, can also occur stratigraphically below or laterally to the Goldstream and Ready Bullion Formations, and were named the Engineer Loess (Holocene) and Gold Hill Loess (>last interglacial). Undifferentiated upland primary loess deposits were known simply as the Fairbanks Loess (e.g. Péwé, 1955, 1975b; Péwé et al., 1966). Since Péwé's initial work, detailed geochronologic and paleomagnetic studies have helped differentiate units present in Fairbanks Loess locales (e.g. Westgate et al., 1990; Oches et al., 1998; Berger, 2003; Lagroix and Banerjee, 2004a; Péwé et al., 2009). Present usage of Péwé's nomenclature finds the terminology generally limited to the Engineer (Holocene; MIS 1), Goldstream (Wisconsinan; MIS 4–2) and Gold Hill (>MIS 5) Formations, but application of the formal names is based on chronology rather than whether the loess is primary or secondary, or present in valley-bottoms or slopes, since the spatial distribution and age of deposits have proven to be more complex (e.g. Begét, 1990; Berger, 2003; Muhs et al., 2003; Lagroix and Banerjee, 2004a,b). The Eva Creek Formation is the formal name Péwé et al. (1997) designated to the forest bed/thaw unconformity that is thought to represent MIS 5e; sediments attributed to other stages of MIS 5 have not been clearly identified in Alaska (e.g. Reyes et al., 2010a). Terminology in this paper will follow recent applications of Péwé's (1975b) formal stratigraphic nomenclature, where divisions are based on the age of the loess rather than location or sedimentology.

The Halfway House site (64.708 N, 148.503 W) is a mid-slope loess deposit mapped as Fairbanks Loess by Péwé et al. (1966) (Fig. 1). Located ~47 km west of Fairbanks, this exposure was created during the construction of the George Parks Highway in the 1960s, and is one of the most extensively studied loess sites in Alaska and the Yukon (e.g. Westgate et al., 1983, 1985; Begét and Hawkins, 1989; Begét, 1990; Begét et al., 1990; Oches et al., 1998; Preece et al., 1999; Vlag et al., 1999; Berger, 2003; Lagroix and Banerjee, 2002, 2004a,b; Muhs et al., 2003, 2008). Collectively, this research indicated that Halfway House is mostly comprised of the Goldstream Formation, and contains a stratigraphic and paleomagnetic record that has regional paleoenvironmental significance. However, poor chronologic control has hindered the interpretation of the record, and made it difficult to compare it to other regional and global paleoenvironmental records. Here we present a tephrostratigraphic framework for Halfway House that provides new chronologic control to this section by identifying several dated tephra beds from other locations in Yukon and Alaska. High-resolution paleomagnetic data provide additional age constraints that support the correlations and new age estimates. Magnetic susceptibility measurements and detailed stratigraphy allow direct correlation of our record to previous studies, placing that research into this new chronologic framework, and provide new insight into Alaskan loess accumulation models.

2. Previous research

2.1. Tephrostratigraphy

Westgate et al. (1983, 1985) first described Halfway House and identified two paleosols and tephra beds across the section. The lowest tephra was correlated to the regionally extensive Old Crow tephra (Fig. 2; OCt; 124 ± 10 ka; Preece et al., 2011a). Preece et al. (1999) describe the second tephra, as well as two additional beds, all stratigraphically above OCt, naming them the Halfway House (HHt), VT and SD tephra beds. At the time, none of these beds had independent age estimates. Muhs et al. (2003) re-examined Halfway House and identified an "unnamed" tephra approximately 1.5 m below OCt and provided several new ages estimates for the Halfway House tephra that suggested an early Wisconsinan age.

2.2. Magnetic susceptibility

Unlike Chinese loess, magnetic susceptibility (χ) in Alaskan loess deposits is lower in paleosols and higher in inorganic loess (e.g. Begét and Hawkins, 1989; Vlag et al., 1999; Liu et al., 2001). There are several generally accepted assumptions that can guide interpretations of changes in magnetic susceptibility in Alaskan loess. First, the dominant fluctuations in susceptibility reflect the size and concentration of magnetic grains present in the loess, although experimental studies examining susceptibility suggest concentration may be more important (e.g. Heider et al., 1996). The amount and size of magnetic grains present in the loess is driven by changes in wind intensity, with highest wind intensities entraining more and/or larger magnetic grains, and carrying them further (e.g. Begét, 1990, 1996, 2001; Vlag et al., 1999). These highest wind intensities may be a result of katabatic winds from ice sheets (Muhs and Budahn, 2006), but may also reflect differences in synoptic climatology during the cold stages (e.g. Mock et al., 1998). These observations indicate that magnetic susceptibility highs occur during cold stages with extensive glaciation, while the lows are associated with intervals of decreased glacier coverage and wind intensity during interglacials or interstadials (e.g. Begét et al., 1990). Second, loess in Alaska is largely glaciogenic, produced by comminution and transported via glacially-fed rivers such as the Tanana, Nenana and Yukon (e.g. Péwé, 1955; Begét, 2001; Muhs et al., 2003; Muhs and Budahn, 2006). High elevation areas of the Alaska Range through St. Elias Mountains host extensive modern glaciers and production and transportation of silt continues today, albeit in a more limited manner (e.g. Muhs et al., 2003, 2004). Therefore, accumulation of loess can be continuous through interglacial–glacial cycles, and paleosols in loess represent periods in time when loess accumulation was sufficiently low that pedogenesis exceeded loess input (e.g. Muhs and Bettis, 2003; Muhs et al., 2004).

Further examination of magnetic mineralogy suggests little pedogenic enhancement of ferrimagnetic content and evidence for some destruction and alteration of magnetic grains, contributing to the lower susceptibility within paleosols (Vlag et al., 1999; Liu et al., 1999, 2001; Begét, 2001). This model of susceptibility variation is also seen in some Siberian loess deposits (e.g. Chlachula et al., 1998;

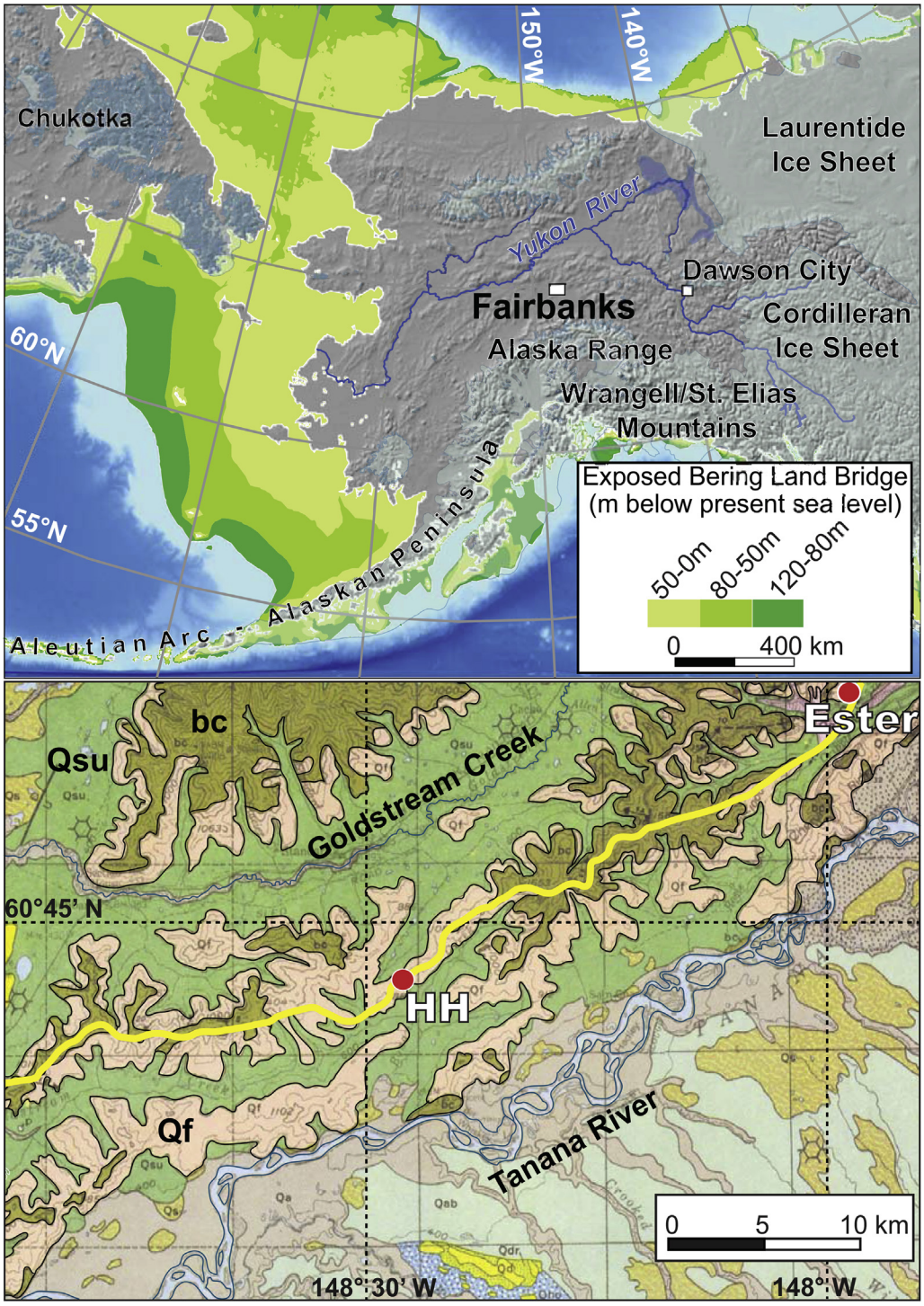

Fig. 1. Location of Halfway House (HH). Top: The rectangle marking Fairbanks encompasses the location of Halfway House, and shows the site relative to the landscape during the last glacial maximum (modified from Froese et al., 2009). Bottom: Location of HH relative to the village of Ester and geologic units of interest. Map is modified from Péwé et al. (1966). Qf- Fairbanks Loess; Qsu-undifferentiated perennially frozen silts; and bc- Birch Creek Schist. Yellow line represents the George Parks Highway.

Evans et al., 2003), with some exceptions (Kravchinsky et al., 2008).

Recognition that magnetic susceptibility in Chinese loess appeared to be highly correlative to benthic foraminiferal $\delta^{18}O$ records (e.g. Heller and Lui, 1986; Kukla et al., 1988) led to a series of studies on Alaskan loess, including the Halfway House section (e.g. Begét and Hawkins, 1989; Begét, 1990, 1996; Begét et al., 1990; Lagroix and Banerjee, 2004a). Assuming a continuous sedimentation rate, results suggested that the site contained a complete record of late- Middle Pleistocene to Holocene loess deposition, and that variations in magnetic susceptibility could be correlated to marine oxygen isotope records. Observations that susceptibility profiles were similar between same-aged sites around the Fairbanks region (e.g. Begét, 1990; Vlag et al., 1999), and statistical tests suggesting significant correlation between isotope

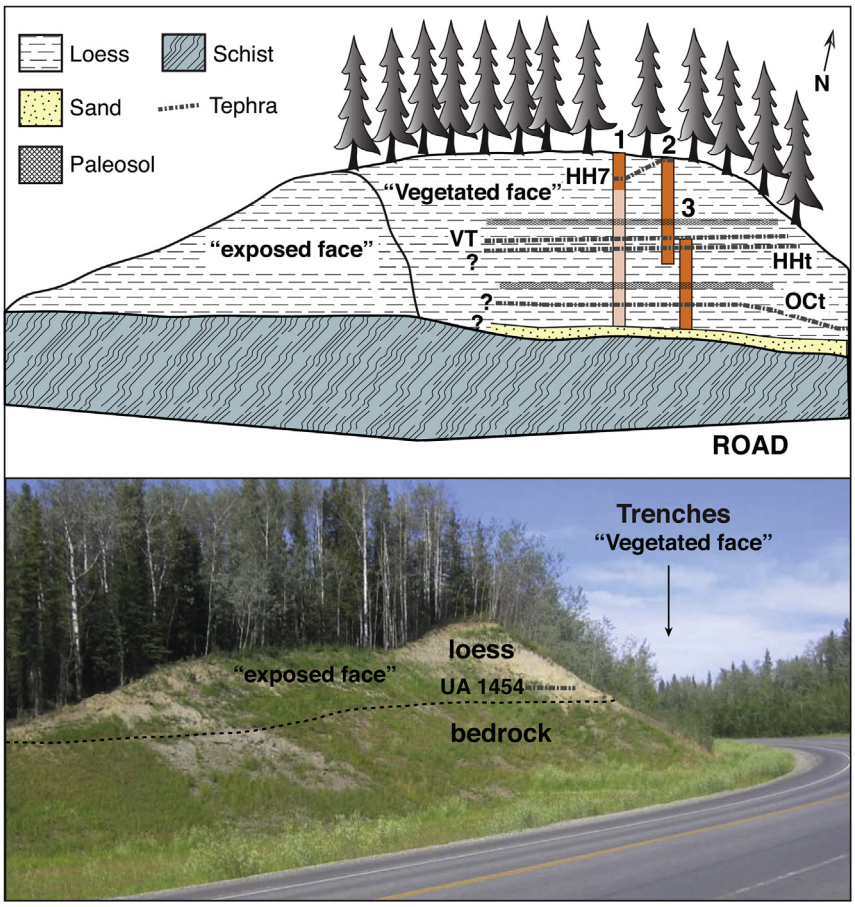

Fig. 2. Halfway House site details. Top: A schematic drawing of Halfway House displaying the most prominent paleosols and continuous tephra beds at the site. Only three trenches were still clearly visible when the site was revisited in 2007. The dark orange highlights the trenches that were logged and sampled over the course of this study. Bottom: A photo of the ~south facing slope of Halfway House, the trenches are on the south-east facing cut, which is heavily vegetated with birch, making it difficult to spot the trenches from the highway. For scale, trench 1 is approximately 12.5 m in height.

records and susceptibility (e.g. Begét and Hawkins, 1989), supported this hypothesis. However, later attempts to refine the chronology at the site with direct age determinations (e.g. luminescence, ^{14}C, ^{10}Be ages) suggested unconformities were present and much of the record was missing (e.g. Berger, 2003; Muhs et al., 2003, 2008).

Lagroix and Banerjee (2002, 2004a,b) used anisotropy of magnetic susceptibility (AMS) to determine regional wind-directions during loess deposition and assess the amount of post-depositional deformation present at Halfway House; their continuous profiles were developed in trench 1 (Fig. 2). They found two zones of post-depositional deformation, 30–40 cm thick, directly above OCt, and associated with the paleosol at ~5–5.5 m (Fig. 3). Implications are that any inclination and declination values obtained from these intervals will not be reliable. Using OCt as their age control, they correlated their magnetic susceptibility curve to SPECMAP. Low susceptibility values directly above OCt (~3.2 m) were interpreted to represent MIS 5e, while paleosols at ~5–5.5 m and ~7.5–8 m were correlated to MIS 5a and a mid-Wisconsinan warm period, respectively. With some modification, this supported Begét's original argument that the record was relatively complete. Results for wind-directions obtained from AMS measurements were placed in the SPECMAP correlated curve, and led them to conclude that wind-directions were predominantly in the N–S direction during interglacials and NW–SE during glacials.

2.3. Age control

Oches et al. (1998) were the first to attempt to date the site using thermoluminscence (TL). They made detailed magnetic measurements and obtained 19 TL dates through trench 1 (Figs. 2 and 3; Oches et al., 1998; Vlag et al., 1999). The TL ages are stratigraphically consistent from the base of the Holocene soil to ~10 m, but below this point the ages become highly variable (Fig. 3). They argued, despite the age reversal that is present above the paleosol couplet at ~7.5–8 m, that their ages to ~80 ka, near HHt, are reliable. Berger (2003) reported a weighted mean TL age of 77.8 ± 4.1 ka for VT, calculated from one age from Halfway House and two from the Gold Hill section, placing VT in latest MIS 5a. This age is consistent with Oches et al. (1998) ages from this depth, but as with them, Berger also measured a much older sample above the paleosol couplet.

Muhs et al. (2003, 2008) carried out detailed geochemical analyses of the loess profile at Halfway House. Using a series of geochemical proxies developed to identify paleosols and assess the amount of weathering (e.g. Muhs et al., 1998, 2003, 2008), they identified up to seven paleosols, but only two displayed an amount of development comparable to the modern soil, corresponding to the paleosol couplet at ~7 m and the paleosol at ~5 m (Fig. 4). Muhs et al. (2008) concluded, based on non-finite ages on charcoal from these paleosols, and the presence of OCt, that the paleosol at ~5.25 m mostly likely formed during the last interglacial, and the

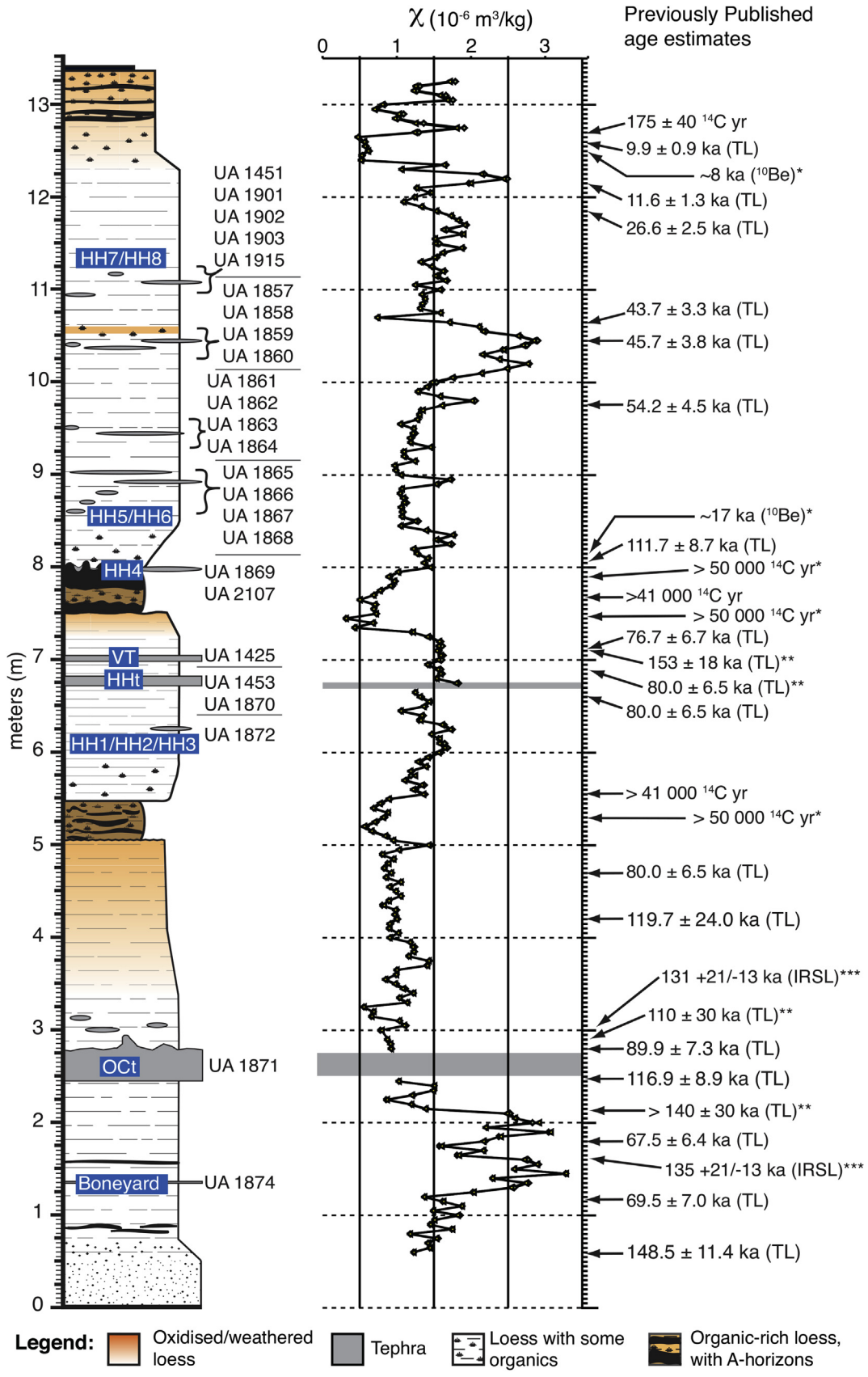

Fig. 3. Stratigraphic log of Halfway House with magnetic susceptibility (χ) measurements (this study) and ages obtained from previous work. Stratigraphy and χ correlate well between studies, allowing accurate placement of ages. *No asterisk* = Oches et al. (1998); *one asterisk* = Muhs et al. (2008); *two asterisks* = Berger (2003); *three asterisks* = Auclair et al. (2007). UA #'s are laboratory numbers assigned to tephra field samples. Note the highly variable age estimates below 8 m.

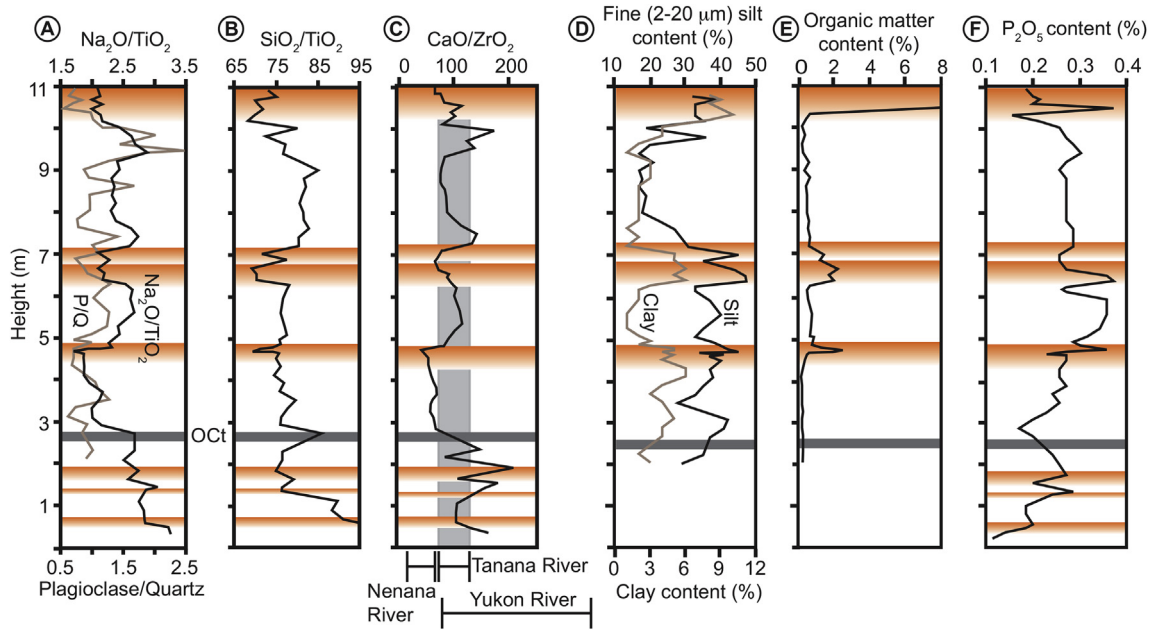

Fig. 4. Selected geochemical profiles modified from Muhs et al. (2003, 2008). A,B- Depletion of Na_2O and SiO_2 track the weathering of plagioclase, reflected in the plagioclase:quartz (P:Q) ratio, confirming a relatively significant degree of weathering associated with the modern soil, the paleosol couplet at ~7 m, and the paleosol at ~5 m. C- Loess at Halfway House appears to be sourced mostly from Tanana river silt, but some input from Nenana and Yukon rivers is probable (Muhs and Budahn, 2006). D- Since clay abundance tracks silt abundance, the variations are likely the results of direct deposition because silt is not a product of pedogenesis. Therefore, peaks of silt and clay within paleosols represent lower wind intensities resulting in deposition of finer material. E– Only the most prominent paleosols at Halfway House show any notable amount of organic material. F- Phosphorous accumulates in organic matter that is present in the A/O horizon of a soil, but is depleted in the B-horizon by plants. This "high-low" trend of phosphorous has not been documented in tundra soils, but is present in the modern soil (i.e. boreal forest) and in the two main paleosols.

couplet likely formed during an early to mid-Wisconsinan interstadial (i.e. >50 ka cal yr BP), an assessment consistent with Berger (2003) and Oches et al. (1998) (Fig. 3).

Auclair et al. (2007) experimented with infrared stimulated luminescence (IRSL), an optical luminescence method, and tested their modifications to the method by dating sediments bracketing OCt. Their ages of 131 + 21/−13 ka and 135 + 21/−13 (Fig. 3) suggested that their approach was more reliable than TL with loess older than 80 ka (Auclair et al., 2007). Further testing of the IRSL method using samples bracketing OCt provided similar ages, but more importantly suggested that there was no hiatus in loess deposition over this time (Roberts, 2012). Jensen et al. (2011) collected samples closely bracketing VT tephra to apply recent advances in the IRSL approach of Auclair et al. (2007). Evidence at other sites where VT is present indicated that the latest MIS 5a age assigned to the tephra was likely too young. Using single-aliquot regenerative-dose (SAR) IRSL, a new age of 106 ± 10 ka was determined for VT, which is consistent with paleoenvironmental and age data from correlative sites (Jensen et al., 2011). This new age suggests that the early mid-Wisconsinan age assigned to the paleosol couplet was also too young.

3. Methodology

3.1. Stratigraphy

Initial studies by Westgate et al. (1983, 1985) and Begét and Hawkins (1989) were completed while the road cut was still well exposed. Later research required excavation of several trenches as the section became re-vegetated (Fig. 2). In 2007, we re-excavated a 3 m section in trench 2 to collect bracketing luminescence samples around VT (c.f. Jensen et al., 2011). This trench was chosen as it had the best exposure of the tephra and was the location where Berger (2003) collected his samples. All of trenches 2 and 3 were re-excavated in 2010 for high-resolution paleomagnetic and tephra sampling. The upper section of trench 2 does not have a modern soil profile, thus to ensure a continuous sampling profile to the present, the upper ~3 m of trench 1 was also re-excavated and sampled.

3.2. Paleomagnetic sampling and analyses

Magnetic susceptibility and remanence samples were collected by pushing 2.5 cm diameter plastic cylinders horizontally into the vertically excavated trenches at 5 cm intervals. Sample orientation was measured with a Brunton compass, set for local declination. A total of ~300 samples were collected. Remanence measurements were made at the University of Alberta by a horizontal 2G Enterprises DC-squid cryogenic magnetometer equipped with an alternating-field (AF) demagnetizer. Samples were progressively demagnetized using up to 16 steps and a maximum field of 100 mT. Results were interpreted with the aid of orthogonal vector component plots and principal component analyses using paleomagnetic software PMGSC developed by Enkin et al. (2000) Magnetic susceptibility measurements were made on a Bartington MS-2 susceptibility meter in three orthogonal orientations (x, y, z), averaged and normalized by mass; both low (0.465 kHz) and high frequency (4.65 kHz) measurements were made, with the former plotted on Figs. 3, 11, 13 and 14 (all measurements available in Supplementary Data).

3.3. Tephra analyses

Tephra samples were sieved into multiple size fractions; those with the most abundant glass were utilized for analysis. The majority of samples collected in this study, with the exception of OCt, VT and HHt, were small and fine, and the size fraction used was 45–75 μm. Details on preparation methods can be found in Jensen

et al. (2008, 2011). Major-element geochemistry was determined on single glass shards with a JEOL 8900 superprobe at the University of Alberta microprobe laboratory using a 15 KeV voltage, 10 μm beam diameter, and 6 nA current. A Lipari obsidian (ID 3506) and OCt were run concurrently with all samples to assure proper calibration and allow accurate comparison between samples run at different times. All data presented are normalized to 100% and individual analyses are available in Supplementary Data.

4. Results

4.1. Stratigraphy

The stratigraphic log is a composite from trenches 1, 2, and 3 (Fig. 3). Trench 3 was logged and sampled from the base of the section to HHt, and this tephra was used to correlate trench 3 to trench 2. The top of trench 2 corresponds to ~11 m in the composite stratigraphic log (Fig. 3). The remainder of the section was logged in the upper 2.5 m of trench 1.

The basal sands that drape the schist bedrock at Halfway House (e.g. Westgate et al., 1983) were exposed, but the bedrock was not. The first paleomagnetic sample was collected directly above the contact between the loess and sand, and from this sample to ~0.70 m, the loess contains small sand beds and concretions. Loess from the sands to ~1.6 m is tan-brown and appears laminated, with thin beds of organic-rich silts. Small sand beds and laminations suggest this basal "loess" may be reworked to some extent, potentially by water. From 1.6 m to 3.4 m the loess is massive, inorganic and displays heavy mottling defined by irregularly oxidized loess. This mottling is a common feature of the drier primary loess deposits in the region and is likely related to past permafrost thaw. Beyond the oxidation, colors are more typical of unaltered loess, generally around 2.5 Y 5/2 (e.g. Muhs et al., 2008). Similar to Muhs et al. (2003, 2008), no morphological evidence of paleosol formation was noted around OCt in trench 3 (~2.5 m), in contrast to the reports of Oches et al. (1998) and Lagroix and Banerjee (2002) (Fig. 5B) in trench 1.

At ~3.4 m the loess becomes more weathered in appearance, taking on an orange tone that deepens moving towards the paleosol at 5 m. By 4.4 m, 0.25–1 cm thick bands of mm-scale silt/clay concretions are cross-cutting through the loess, and the loess itself has become friable and carries a deep orange hue. Munsell colors through this section tend to have hues of 7.5 YR–10 YR with high chromas and values (Fig. 5D). The paleosol (~5–5.4 m) is expressed as a cryoturbated organic-rich silt bed comprised of cryoturbated and weathered humic horizons and charcoal. The upper contact grades into less weathered loess, but occasional humic lenses are present. The loess becomes 'speckled' approaching HHt at ~6.7 m. The speckles are generally <1 mm diameter, often circular but occasionally linear and up to a few centimeters in length, weakly developed, and appear to be composed of Fe (and/or Mn). Some of these 'speckles' are likely rhizoliths, the remains of grass and shrub roots that oxidized following permafrost thaw. The loess is mottled and oxidized around HHt and VT, but remains massive and inorganic to the base of the paleosol couplet (Fig. 5C). The couplet is ~50 cm thick, with a poorly expressed B-horizon at its base. It is comprised of a lower, 10–20 cm thick, A-horizon intercalated with organic-rich silt, overlain by a ~10 cm thick less organic-rich B-horizon, and capped by another A-horizon/organic-rich silt bed that is 20–30 cm thick. Charcoal is abundant, the upper contact is highly undulatory, and the couplet rises and thickens slightly towards the right end of the trench (Figs. 3 and 5C). Except for two oxidized intervals, one ~50 cm above the paleosol couplet, the other at ~10.5 m, which may in fact be a weak B-horizon, the loess is massive and inorganic for the remainder of trench 2.

Trench 1 was logged and sampled from the modern soil to ~2.5 m below the surface, the base approximately 10–20 cm below a series of small tephra samples that correlate to those found at the top of trench 2 (Fig. 5B). Loess is massive and inorganic into the base of the modern soil, of which the B-horizon becomes visible ~1 m below the surface. The soil is a complex of several interbedded O, A and B-horizons, rich in charcoal, with a prominent organic bed visible ~50–60 cm below the surface (Fig. 5A).

4.2. Revised tephrostratigraphy

Muhs et al. (2003, 2008) label an "unidentified tephra" below OCt in their stratigraphic logs, and this bed likely corresponds to a sample collected at ~1.5 m, a continuous, yellow-white bed up to 0.5 cm thick (Fig. 3; UA 1874). This tephra has been correlated to the Boneyard tephra, first identified at the Palisades site on the Yukon River, ~250 km west of Fairbanks, but also present at a new Gold Hill Loess exposure near Ester (Table 1, Fig. 6; Jensen et al., 2013). It has distinctive major-element glass geochemistry and morphology, with relatively high Al_2O_3 weight percent (wt%) and low FeO_t wt% compared to other Yukon–Alaska tephra beds at this SiO_2 wt % range. Glass morphology of the bed consists almost entirely of blocky, thick-walled pumice that have small evenly distributed vesicles and abundant phenocrysts and microlites.

OCt (UA 1871), ~1 m above Boneyard tephra, is 20–40 cm thick, has a sharp lower contact, a heavily cryoturbated upper contact, and includes pods of tephra up to 20 cm above the main deposit (Figs. 3 and 5). It is a rhyolitic tephra bed with few phenocrysts and a glass morphology predominantly consisting of platy glass and thick-walled pumice (Fig. 6; for a detailed review see Preece et al., 2011a).

Preece et al. (1999) characterize a thin and discontinuous tephra within "a dark silt that has been deformed by solifluction" approximately 3 m above Old Crow and 1.5 m below HHt and VT, which they subsequently named SD tephra. Despite a tentative identification of this tephra in the same stratigraphic location by Lagroix et al., 2004, we were unsuccessful in recollecting this tephra. Given the stratigraphy described by Preece et al. (1999) and Lagroix et al. (2004), we suggest that this tephra is present within the paleosol described here at 5–5.4 m.

HH1, HH2 and HH3 were identified from a single sample (UA 1872) collected on a face that was cleared between trenches 2 and 3 to track HHt. Approximately 50 cm below HHt, it was comprised of several white, diffuse pods, the largest 0.5 cm thick and 7 cm long. Glass morphology of the sample is predominantly thick-walled tricuspate and bubble-wall shards, although conspicuous shards of frothy pumice are present. Major-element geochemical analyses reveal that three separate populations are present. HH1 is the predominant population, comprised of tricuspate and bubble-walled shards, with a distinct geochemical trend that ranges from low SiO_2 wt% dacite to high SiO_2 wt% rhyolite. This tephra has been correlated to the Snag tephra, found in exposures along the White River, Yukon Territory (Tables 1 and 2; Fig. 7; Turner et al., 2013). Supporting this correlation is HH2, the second most abundant population, which is comprised of frothy pumice. HH2 is geochemically similar to, but can be distinguished from, the Sheep Creek-Canyon Creek tephra (Fig. 7; SC-CC; e.g. Westgate et al., 2008). HH2 has been correlated to a previously unreported tephra bed found in the same stratigraphic sequence as Snag at the White River exposure, although as a distinct bed (Jensen, unpublished data). For ease of discussion, we name this tephra informally as "White River-unknown 5" (WR-UN5), to remain consistent with nomenclature of Turner et al. (2013). The HH3 population is recognized from 5 shards in this sample, but is common as detrital material in virtually all samples collected stratigraphically above,

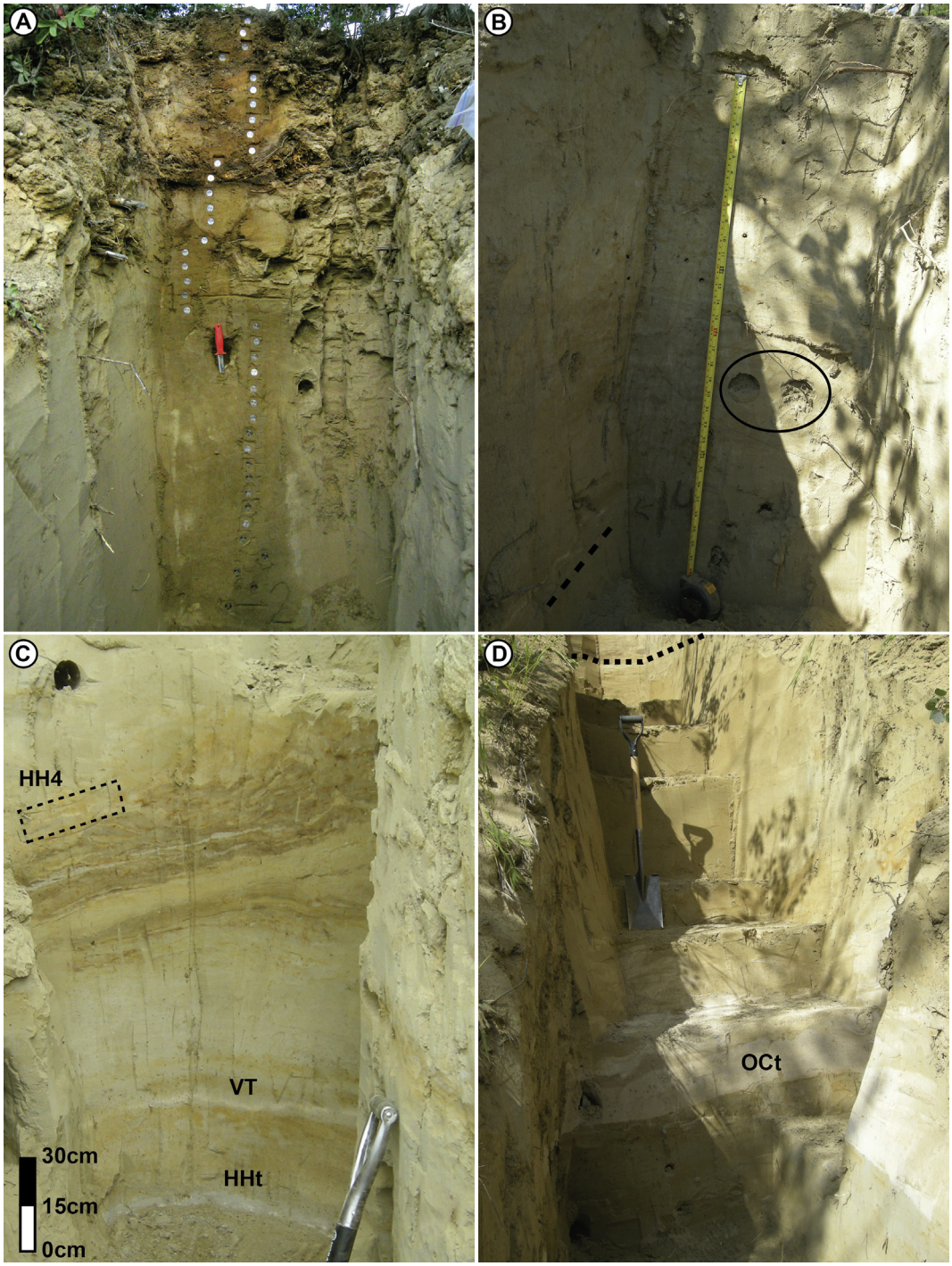

Fig. 5. Important features of Halfway House. A- Paleomagnetic samples collected at 5 cm intervals in the upper ~2.5 m of trench 1. The modern soil complex consists of several interbedded A and B- horizons. Scale, knife = 20 cm. B- The top of trench 2, two holes are visible and likely remnants from Oches' TL sampling. The wisps of tephra defined by the dashed line are part of the HH7/HH8 complex and correlate the two trenches. Scale, measuring tape = 80 cm. C- The paleosol couplet above VT and HHt, the 5 cm paleomagnetic sampling profile was partially collected through the face with HH4. D- OCt, up to 40 cm thick, is within grey-tan loess, while the loess above OCt to the paleosol (base at dashed line) is weathered, displaying an orange-hue. Scale, shovel = 1.25 m.

but not below, this level. HH3 has been correlated to samples (UA 1624/1909; Fig. 7) collected ~15–20 cm below VT at Gold Hill IV (for location details see Evans et al., 2011), where it is a mm-scale bed, semi-continuous, within heavily oxidized and laminated loess. It is a high SiO_2 wt% rhyolite with distinctly low K_2O wt% (Table 1; Fig. 7). Only three beds of similar composition are known: the Donjek, Kulukak Bay and Stampede tephras. The Donjek and Kulukak Bay tephras have higher K_2O wt%, and the Kulukak Bay tephra is above VT (Kaufman et al., 2001; Jensen et al., 2011; Turner et al., 2013). However, glass major-element geochemistry of HH3 and averages of the Stampede tephra presented by Begét and Keskinen (1991) are notably similar (Tables 1 and 2; Fig. 7). The Stampede tephra was first documented within a block of silt that is faulted and folded into a push moraine associated with the Lignite

Table 1
Major-element glass geochemistry of tephra beds from Halfway House.

Sample		SiO_2	TiO_2	Al_2O_3	FeO_t	MnO	MgO	CaO	Na_2O	K_2O	Cl	H_2O_{diff}	n
Boneyard	MEAN	76.15	0.04	14.21	0.60	0.14	0.10	1.04	3.94	3.69	0.10	7.40	45
	STDEV	0.28	0.04	0.30	0.22	0.03	0.03	0.08	0.47	0.50	0.05	0.81	
Old Crow	MEAN	75.47	0.31	12.85	1.76	0.08	0.30	1.51	3.72	3.71	0.28	3.34	18
	STDEV	0.18	0.04	0.10	0.06	0.03	0.03	0.06	0.16	0.09	0.02	1.29	
HH1	MEAN	71.27	0.64	14.20	3.02	0.05	0.68	2.18	4.14	3.71	0.10	4.29	32
	STDEV	3.44	0.36	0.78	1.32	0.04	0.45	1.07	0.32	0.65	0.03	1.90	
HH2	MEAN	75.13	0.19	14.35	1.24	0.04	0.36	1.67	4.07	2.92	0.03	5.22	12
	STDEV	0.80	0.06	0.53	0.12	0.03	0.09	0.38	0.31	0.22	0.02	2.19	
HH3	MEAN	76.78	0.25	13.22	1.50	0.10	0.34	1.72	4.47	1.49	0.16	6.52	59
	STDEV	0.42	0.04	0.16	0.06	0.04	0.03	0.08	0.28	0.06	0.03	1.79	
HHt	MEAN	73.04	0.48	14.16	2.49	0.14	0.54	1.99	5.17	1.86	0.14	2.31	84
	STDEV	1.47	0.09	0.44	0.56	0.03	0.16	0.50	0.27	0.11	0.02	1.40	
VT	MEAN	70.51	0.58	14.83	3.17	0.10	0.69	2.47	4.57	2.92	0.16	2.52	79
	STDEV	1.36	0.08	0.41	0.49	0.03	0.20	0.42	0.21	0.21	0.04	1.66	
HH4	MEAN	73.07	0.20	15.56	1.46	0.05	0.46	2.10	4.43	2.63	0.04	5.77	29
	STDEV	0.69	0.05	0.47	0.13	0.03	0.06	0.17	0.16	0.14	0.02	2.57	
HH5	MEAN	70.60	0.69	14.56	3.19	0.07	0.68	2.30	4.33	3.48	0.11	2.55	48
	STDEV	1.43	0.17	0.33	0.55	0.03	0.20	0.51	0.30	0.30	0.06	1.59	
HH6	MEAN	75.88	0.27	13.04	1.34	0.05	0.19	0.88	3.73	4.53	0.11	6.04	73
	STDEV	0.53	0.05	0.23	0.13	0.03	0.05	0.15	0.16	0.13	0.03	1.52	
HH7 pop.1	MEAN	78.57	0.12	12.41	0.87	0.06	0.18	1.03	3.27	3.28	0.20	6.29	81
	STDEV	0.47	0.04	0.37	0.09	0.03	0.05	0.11	0.24	0.32	0.04	1.05	
HH7 pop.2	MEAN	76.79	0.14	13.47	1.04	0.06	0.28	1.68	3.83	2.56	0.15	4.59	25
	STDEV	0.34	0.04	0.19	0.09	0.03	0.05	0.13	0.16	0.14	0.04	1.90	
HH7 all	MEAN	78.15	0.13	12.66	0.91	0.06	0.21	1.18	3.40	3.11	0.19	5.89	106
	STDEV	0.88	0.04	0.56	0.12	0.03	0.07	0.30	0.33	0.42	0.04	1.48	
HH8	MEAN	74.24	0.28	13.54	2.12	0.08	0.23	1.27	4.44	3.58	0.23	4.60	9
	STDEV	0.27	0.05	0.18	0.15	0.02	0.05	0.12	0.37	0.14	0.04	2.19	

Data normalized on a water-free basis. FeOt = total Fe as FeO; H_2Odiff = water by difference; n = number of analyses.
Boneyard = UA 1874; Old Crow = UA 1871; HH1 = UA 1872; HH2 = UA 1872; HH3 = UA 1872, 1857–69, 1873, 2107.
HHt = UA 1870, 1453; VT = UA 1425; HH4 = UA 1869, 2107; HH5/6 = UA 1857–1868, 1873; HH7 = UA 1901–3, 1915, 1451.
HH8 = UA 1901.
Correlations: HH1 = Snag; HH2 = WRUN5; HH3 = Potential Stampede; HH4 = SCt-K; HH5 = DAB; HH6 = DCt; HH8 = Dawson.

glaciation, and a site comprised of interbedded sand and silt on Richardson Highway by the Tanana River. The Lignite glaciation is thought to be correlative to the nearby Canyon Creek vertebrate locality (Weber et al., 1981; Begét and Keskinen, 1991). The tephra was subsequently correlated the Goose Bay tephra in the Cook Inlet region (Reger et al., 1996). Age estimates for the Stampede tephra, based on stratigraphy, $^{40}Ar/^{39}Ar$ and TL dating, range widely from >140 ka to ~380 ka (Begét and Keskinen, 1991; Reger et al., 1996; Begét, 2001). However, recent cosmogenic ages (^{10}Be) reported by Dortch et al. (2010) suggest that the Lignite Glaciation may have had an advance in MIS 5d, and the presence of *Bison priscus* fossils at Canyon Creek suggest this site must be Rancholabrean in age, thus likely ≤MIS 6 (e.g. Westgate et al., 2008). These new age constraints support the correlation, although analyses with reference material of the Stampede tephra are still required.

HHt (~6.7 m; UA 1453, 1870) and VT (~7 m; UA 1425) are discrete beds up to 10 and 3 cm thick, respectively. Both tephra beds have diffuse contacts, but similar to OCt and Boneyard tephra, they can be traced continuously across the exposure, suggesting minimal post-depositional disturbance (Fig. 5). Both tephra beds are mainly rhyolitic, but contain some dacitic shards, although the latter are more abundant in VT (Fig. 6, Table 1). Glass morphology of both tephra beds is comprised of bubble-walled and tricuspate shards with some pumice, although HHt glass is much thicker-walled. Detailed descriptions and geochemistry of HHt and VT are in Preece et al. (1999) and Jensen et al. (2011, 2013).

HH4 (UA 1869, UA 2107) was collected at the contact between the paleosol couplet and overlying loess (Figs. 3 and 5C). The samples consist of diffuse blebs up to 1 cm thick that were semi-continuous for 70 cm across the trench. HH4 is very fine, most glass is <75 μ, and consists of frothy pumice. Geochemical analyses show abundant detrital glass shards that have very low Na_2O and high SiO_2 concentrations. This suggests they are heavily weathered, which would make them particularly susceptible to Na-loss during analyses. The unweathered shards form a coherent population that has distinct glass geochemistry and morphology that places it in the Sheep Creek family (c.f. Westgate et al., 2008). Concurrent analyses with reference material show that HH4 correlates to Sheep Creek-Klondike (SCt-K, ca. 80 ka; Westgate et al., 2008; 77–81 ka; Demuro et al., 2013) (Tables 1 and 2; Fig. 7). SCt-K is a widely distributed tephra bed in the Klondike region south of Dawson City, Yukon (Fig. 1), and is consistently found directly above a paleosol (Sanborn et al., 2006; Schweger, 2003; Westgate et al., 2008).

Thirteen samples were collected above SCt-K; a series of discontinuous blebs and thin beds of tephra, rarely greater than 0.2 cm thick, were collected at intervals to the top of trench 2 (Figs. 3 and 5B). Several small samples were also collected between 2.2 and 2.5 m below the surface in trench 1. Most samples only contained glass in the 45–75 μ fraction. Analyses revealed abundant detrital material, and in all samples but those collected around ~11 m (i.e. UA 1915 at the surface in trench 2, and most samples in trench 1), it was difficult to discern any predominant geochemical population in any one sample. However, taken collectively, we were able to isolate several distinct geochemical populations within the samples. HH5 and HH6 comprise two of the largest populations that were not correlated to older, known tephra beds, such as HH3 (potential Stampede tephra correlative), OCt and HHt. To test if contamination during laboratory processes may have mixed the samples, several from different stratigraphic levels were re-processed and analyzed, to obtain the same result. In consideration of prior stratigraphic knowledge and initial results, reference samples of the Dominion Creek tephra (DCt; Preece et al., 2000, 2011b) and Dome Ash Bed (DAB; e.g. Péwé, 1975b; Preece et al., 1999) were analyzed with the re-processed samples. The major-

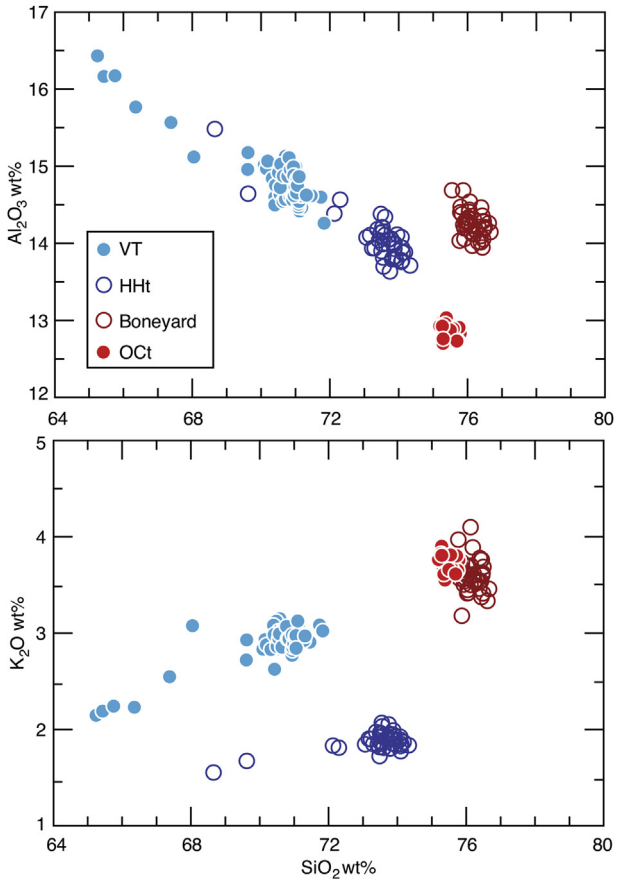

Fig. 6. Selected bivariate plots of major-element glass geochemistry of tephra beds previously reported at Halfway House.

element glass geochemistry permits correlation between HH5 and DAB, and HH6 and DCt (Table 1; Fig. 8). Additionally, UA 1454, a single sample collected from the exposed face at Halfway House (Fig. 2), 4 m below the surface, and 4 m above the bedrock contact, also correlates to HH5 and DAB. This sample contains no other populations, and indicates that DAB is present at the site as a primary bed (Fig. 8). The correlation of DCt to HH6 is supported by the stratigraphy. At all locations where DCt has previously been collected, it is consistently found 30–100 cm above SCt-K (e.g. Preece et al., 2000; Westgate et al., 2008). The stratigraphy of DAB is less certain; although originally placed within the Eva Creek Formation (e.g. Péwé et al., 1997), Muhs et al. (2008) show it likely post-dates MIS 5e, but is associated with non-finite radiocarbon ages, thus it remains uncertain if DAB is within later MIS 5 or early MIS 4 loess.

HH7 was collected 5–10 cm from the surface in trench 2 (UA 1915), a pink-grey bleb up to a 1 cm thick and 5 cm long. This sample correlates to UA 1451, 1902 and 1903 in trench 1, pink wisps up to 0.5 cm thick and up to 10 cm long, linking the two trenches (Fig. 9). HH7 is a high SiO_2 wt% rhyolite consisting of two main populations (Table 1; Fig. 9). HH7 has been correlated to three other sites around the Fairbanks area; Eva Creek, Gold Hill, and remnants of the Engineer Creek/Dawson Cut exposures near the junction of the Steese Highway and Gold Mine Trail Road (Fig. 9; for location details see Péwé et al., 2009). At all sites this tephra bed is a thin but semi-continuous wisp, within inorganic loess and generally 1–2.5 m beneath the local surface. Glass morphology is also consistent across all samples, predominantly comprised of chunky glass shards and pumice that is rich in phenocrysts and microlites, complicating analyses. Repeated observations of two geochemical populations that are on trend with each other in samples from several sites suggests that HH7 is the product of one complex eruption. HH7 bears a striking resemblance to both the Chatanika and EB tephras (Table 2; Fig. 9). Chatanika tephra was formally named by Péwé (1975b), and is described as a 1–10 mm thick white vitric ash, consistently found at sites in the upper portions of the Goldstream formation, with a type section designated at the Chatanika River, 40 km north of Fairbanks. EB tephra has only been found at Eva Creek (on "Eva Bench"), near the base of what has been mapped as Engineer Loess (Péwé et al., 2009). Glass morphology of HH7, Chatanika, EB are similar, particularly notable is the

Table 2
Major-element glass geochemistry of reference samples.

Sample		SiO_2	TiO_2	Al_2O_3	FeO_t	MnO	MgO	CaO	Na_2O	K_2O	Cl	H_2O_{diff}	n
Snag	MEAN	68.17	0.99	14.63	4.30	0.07	1.13	3.12	4.38	3.15	0.08	1.55	39
	STDEV	2.88	0.25	0.66	1.09	0.02	0.54	0.99	0.23	0.52	0.02	2.17	
WRUN5	MEAN	68.17	0.99	14.63	4.30	0.07	1.13	3.12	4.38	3.15	0.08	1.55	39
	STDEV	2.88	0.25	0.66	1.09	0.02	0.54	0.99	0.23	0.52	0.02	2.17	
Stampede*	MEAN	77.23	0.23	13.30	1.34	–	0.34	1.66	4.30	1.46	0.15	3.97	54
	STDEV	0.29	0.06	0.15	0.11	–	0.03	0.08	0.16	0.05	0.04	0.86	
SCt-K	MEAN	72.87	0.21	15.56	1.46	0.04	0.50	2.21	4.58	2.53	0.04	4.09	59
	STDEV	0.46	0.04	0.22	0.11	0.03	0.06	0.15	0.23	0.12	0.02	1.98	
DAB	MEAN	71.43	0.55	14.46	2.67	0.05	0.50	1.86	4.61	3.76	0.10	3.24	20
	STDEV	0.53	0.07	0.19	0.19	0.03	0.06	0.16	0.12	0.10	0.02	1.76	
DCt	MEAN	75.74	0.28	13.05	1.30	0.04	0.19	0.90	3.82	4.59	0.10	5.79	43
	STDEV	0.57	0.06	0.26	0.12	0.03	0.04	0.17	0.13	0.12	0.02	1.82	
Chatanika**	MEAN	76.90	0.13	13.52	1.01	0.08	0.29	1.65	3.78	2.57	0.15	6.01	7
	STDEV	0.13	0.13	0.17	0.06	0.02	0.02	0.15	0.13	0.13	0.02	1.75	
EB**	MEAN	77.62	0.12	13.06	0.83	0.08	0.17	1.26	3.63	3.01	0.22	6.25	12
	STDEV	0.86	0.08	0.58	0.12	0.04	0.07	0.22	0.22	0.23	0.07	2.10	
Chatanika	MEAN	76.67	0.13	13.47	0.99	0.05	0.29	1.54	3.78	2.90	0.19	6.37	23
	STDEV	0.72	0.04	0.67	0.15	0.03	0.13	0.31	0.32	0.52	0.08	1.81	
EB	MEAN	77.60	0.11	12.98	0.89	0.06	0.23	1.17	3.58	3.20	0.19	6.69	16
	STDEV	1.13	0.03	0.86	0.16	0.03	0.13	0.33	0.46	0.51	0.03	0.79	
Dawson	MEAN	74.08	0.27	13.65	2.05	0.07	0.22	1.24	4.52	3.68	0.22	3.67	39
	STDEV	0.26	0.04	0.16	0.07	0.03	0.03	0.06	0.21	0.11	0.03	2.25	

Data normalized on a water-free basis. FeOt = total Fe as FeO; H_2Odiff = water by difference; n = number of analyses.
*Values from Begét and Keskinen (1991) **Values from Péwé et al. (2009). Snag = UA 1589; WRUN5 = UA 1930, 1928.
SCt-K = UT 40; DAB = UT 745; DCt = UT 1905; Chatnika = UT 2178; EB = UA 357; Dawson = UA 1000.
HH1 = Snag; HH2 = WRUN5; HH3 = Stampede?; HH4 = SCt-K; HH5 = DAB; HH6 = DCt; HH8 = Dawson.

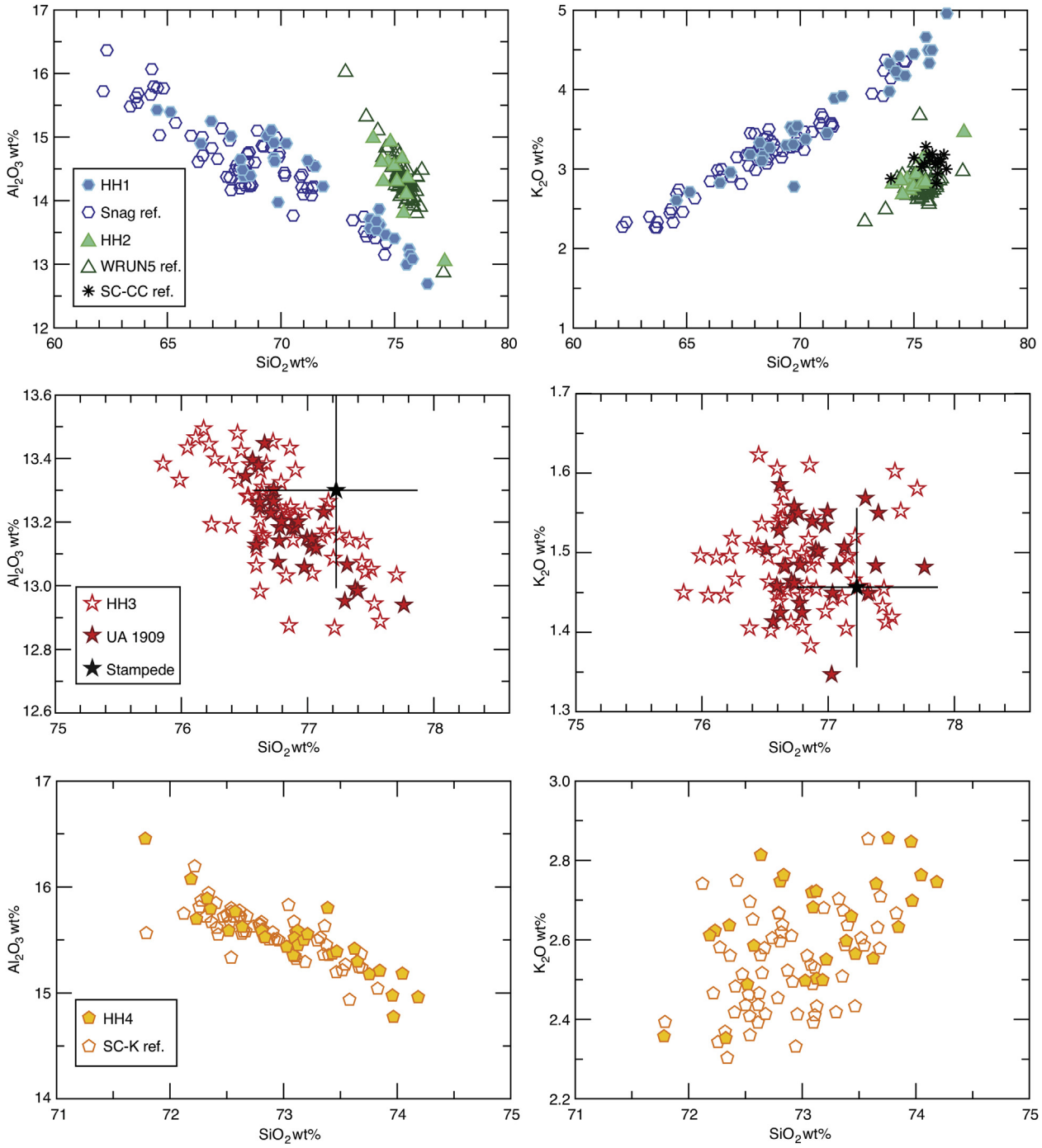

Fig. 7. Selected bivariate plots of major-element glass geochemistry of HH1, HH2, HH3 and HH4 and their correlative beds. Top row: HH1, HH2 and reference material from Snag, WR-UN5, and SC-CC tephra beds. Middle row: HH3 plotted with UA 1909 from Gold Hill IV, and values reported for Stampede tephra (with 2 sigma error bars) from Begét and Keskinen (1991). Bottom row: HH4 plotted with a SC-K reference sample (UT 40).

abundance of microlites in all three. However, analyses of reference EB and Chatanika samples with HH7 were inconclusive. Very little of Péwé's original material remained, thus acquiring enough analyses for a truly meaningful comparison between tephras with a relatively broad compositional range was difficult. Fig. 9 shows that all three tephra are similar to one another, and while EB plots relatively well with the lower SiO_2 population of HH7, Chatanika captures the entire geochemical range Nonetheless, while Chatanika is the more likely correlative, particularly in light of its previously described stratigraphic context, the geochemical data do not preclude the possibility that each tephra is unique, or that all are the same bed.

HH8 (UA 1901) was collected in trench 1 at the same level as HH7. HH8 was a <0.2 mm thick white wisp. This tephra is also largely comprised of detrital glass, and some shards share affinities to older tephra beds at the site. However, the largest single population is a rhyolite that shares many geochemical and glass morphological characteristics to the Dawson tephra. Originally described in the Klondike, Yukon, this well characterized bed is part of a group of geochemically distinct tephra beds that includes OCt,

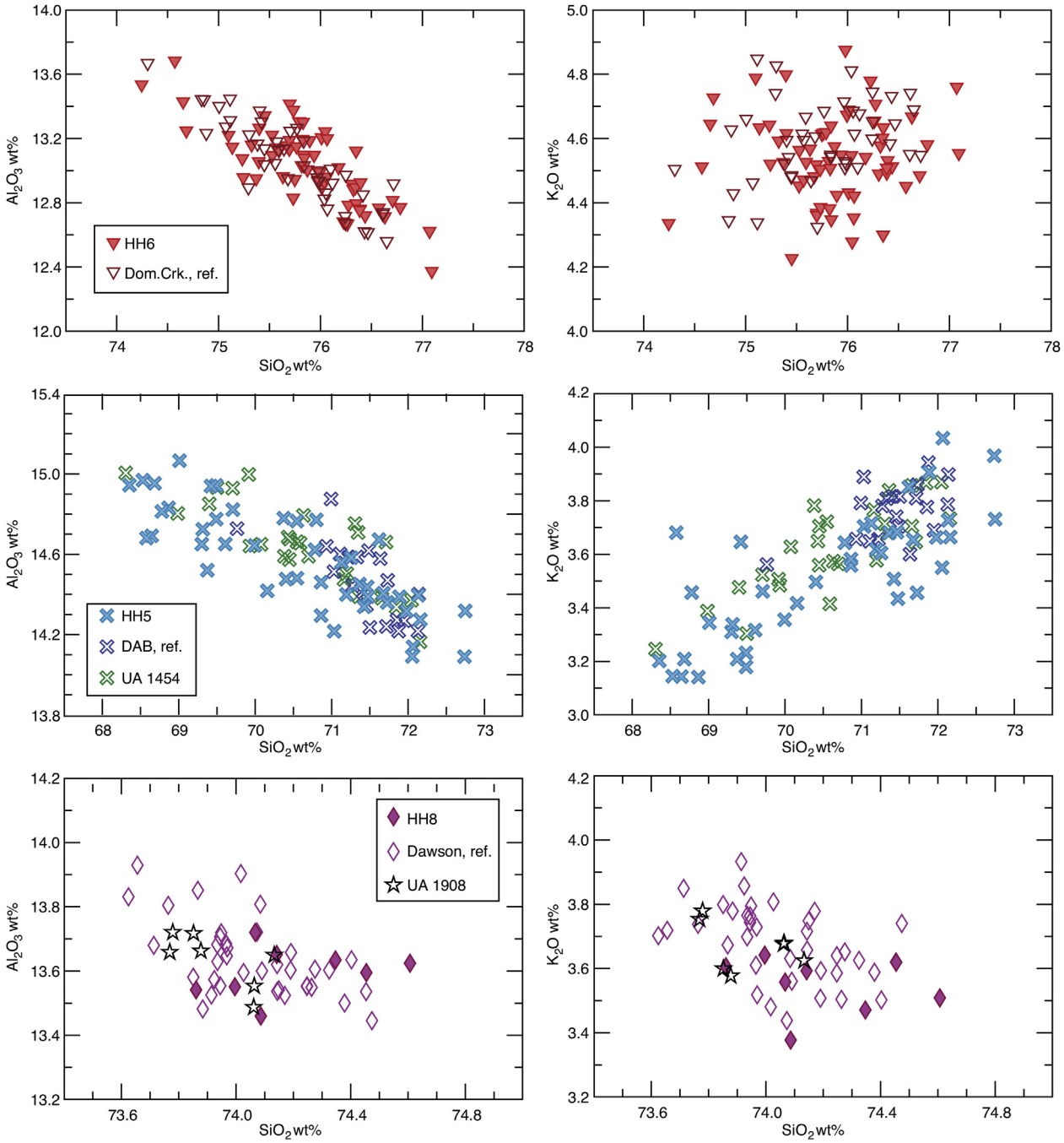

Fig. 8. Selected bivariate plots of major-element glass geochemistry of HH5, HH6, and HH8 and their correlative beds Top row: HH6 and DCt reference material. Middle row: HH5, DAB reference material, and UA 1454. DAB reference contains fewer dacitic shards than HH5 and UA 1454. This may be the result fewer analyses and/or the processing of reference material; during glass flotation (e.g. Jensen et al., 2008), it is possible to lose lower SiO_2 wt% shards if the density of the separation liquid is too low (e.g. Froese et al., 2003). Bottom row: HH8, Dawson reference material and UA 1908, a sample from Gold Hill III.

Togiak Bay and DL tephras (e.g. Preece et al., 2011a). Dawson is the only known bed of this group deposited after MIS 5, around 25,300 ^{14}C yr BP (ca. 30.2 cal ka BP; Demuro et al., 2008). Re-analysis of HH8 with reference material of Dawson tephra, and its stratigraphic position within ~2.5 m of the surface of the exposure, support the correlation (Figs. 3 and 8).

4.3. Loess magnetism

Approximately 300 samples at 5-cm resolution scale were collected for magnetic susceptibility and natural remnant magnetization (NRM) measurements. A minimum of six AF steps, and an average of 11, were used for principal component analyses to obtain characteristic NRM values (ChRM). Many samples carry a secondary magnetic overprint that is removed in the first few demagnetization steps. It has scattered directions unrelated to the present-day field at Halfway House, and is probably a viscous remanence acquired during storage in the laboratory. After removal of the overprint, orthogonal vector end-point plots reveal monotonic decrease towards the origin demonstrating the presence of a stable

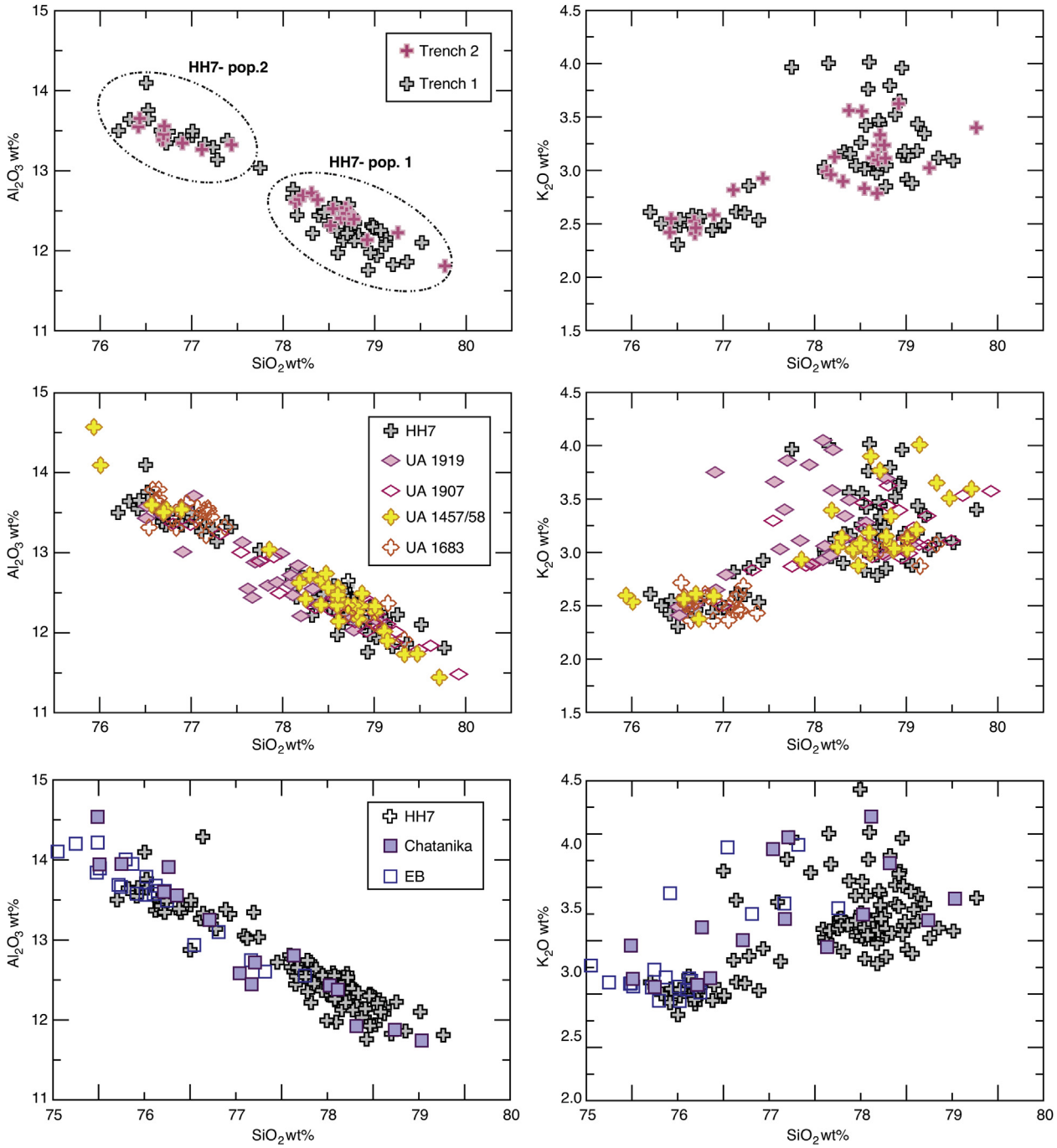

Fig. 9. Selected bivariate plots of major-element glass geochemistry of HH7 and samples from other sites. Top row: Correlation of the uppermost sample in trench 2 to trench 1 (HH7). Middle row: HH7 correlates to other samples in the Fairbanks region: UA 1919 (Gold Hill IV), UA 1907 (Gold Hill III), UA 1457/58 (Eva Creek), UA 1683 (Engineering Creek/Dawson Cut). Bottom row: Reference samples of Chatanika and EB tephra beds plotted with both populations of HH7.

component that we interpret as a record of the ancient geomagnetic field. Some samples exhibit almost ideal behavior (Fig. 10a). For the entire collection, maximum angular deviation (MAD) values are generally very small, with 1st quartile, median, and 3rd quartile values of 0.6°, 1.0°, and 1.8°, respectively. Eight values lie between 5° and 10°. A single outlier of 19.4° was rejected. Demagnetization behavior of representative loess and paleosol samples is illustrated in Fig. 10. The loess (10b) is more magnetic than the paleosol (10c), a pattern that is also found in susceptibility (2.4×10^{-6} m^3/kg for the loess, 0.94×10^{-6} m^3/kg for the paleosol). While there has been some evidence of post-depositional destruction of magnetic minerals (Liu et al., 2001), these variations largely reflect the relative amount of magnetic material present. Lagroix and Banerjee (2002) show that the magnetic mineralogy is dominated by magnetite and/or maghemite, with mass fractions of ~0.3% and ~0.03% in loess and paleosol, respectively. The directional results and susceptibility data are shown as stratigraphic profiles in Fig. 11.

Inclination values recorded in the paleosol at ~7.75 m show a systematic shallowing, with corresponding shifts in declination. MAD values throughout this excursional interval have a mean of

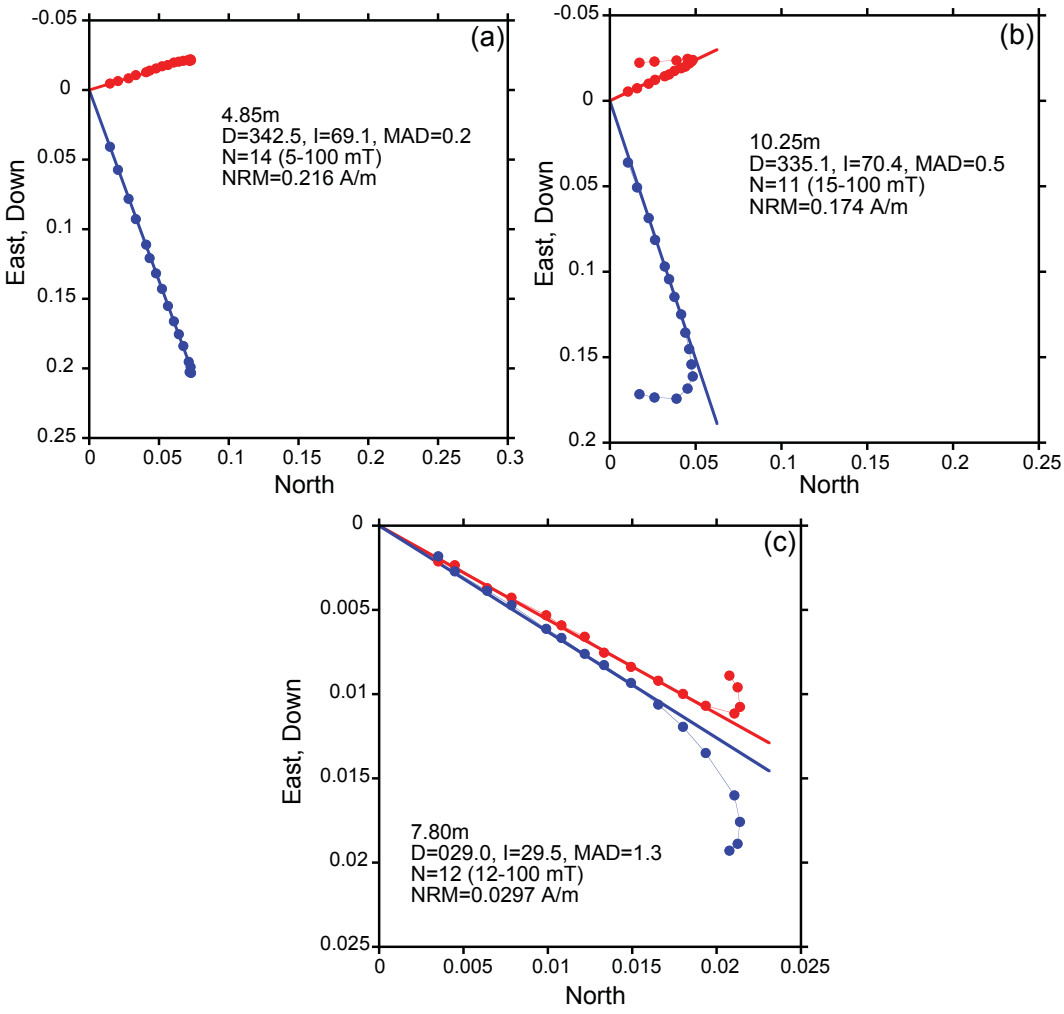

Fig. 10. Orthogonal vector end-point plots. Numerical data given in each plot are stratigraphic height; declination (D), inclination (I) and maximum angular deviation (MAD) (all in degrees); number of demagnetization steps (N), range given in brackets; natural remanent magnetization (NRM). The three samples illustrate (a) almost ideal demagnetization behavior, and examples of (b) loess, and (c) paleosol.

1.4°, and never exceed 2.5° (Fig. 11). Once the low-coercivity overprint is removed, a single underlying magnetic component is found in all samples. There is no evidence for two magnetic signals arising from an original detrital remanence on which is superposed a later component acquired during pedogenesis. There are two options: either the paleosol retains an original detrital magnetic signal, or such a component has been completely lost and replaced by an entirely pedogenic signal. The second option can be rejected on the basis of the results reported by Lagroix and Banerjee (2002) who demonstrate that primary ferromagnetic grains not only survive, but do so in sufficient quantities to faithfully record prevailing wind directions throughout most of the time represented at Halfway House—including the interval spanned by the excursional directions. We conclude that pedogenetic processes have not substantially altered the paleomagnetic directions we observe.

Age control provided by bracketing tephra beds, VT (106 ± 10 ka) and SCt-K (~80 ka), indicate this excursion cannot be attributed to either the Blake (ca. 120 ka; Singer and Hoffman, 2005) or Laschamp (ca. 41 ka; Singer et al., 2009). An extended period from ~100 to 80 ka of low paleointensity and increased productivity in ^{10}Be has been documented in multiple marine cores (e.g. Frank et al., 1997; Guyodo and Valet, 1999; Carcaillet et al., 2004; Channell et al., 2009). This interval also contains a directional excursion, subsequently given the name “post-Blake” (e.g. Thouveny et al., 2004). However, until recently, only one record of a directional excursion had been documented during this interval, from Lac du Bouchet in the French Massif Central (Thouveny et al., 1990). A series of transitionally magnetized flows on Iceland, previously ascribed to the Laschamp (e.g. Levi et al., 1990; Ferk and Leonhardt, 2009), were recently dated to 94 ± 8 ka (Jicha et al., 2011). Jicha et al. (2011) correlate this excursion to the post-Blake, but resurrect the name of Skálamælifell, the original name for the Icelandic excursion before it was erroneously correlated to the Laschamp (Kristja;nsson and Gudmundsson, 1980). The virtual geomagnetic poles (VGPs) for the observed low-inclination directions at Halfway House trace out a trajectory (Fig. 12) towards a group of Icelandic VGPs in northwest Africa reported by Kristjánsson (2003) and confirmed by Ferk and Leonhardt (2009). Kristjánsson (2003) suggests that these divergent VGPs “possibly” belong to the Skálamælifell excursion. Ferk and Leonhardt (2009) concur, but suggest a much larger VGP loop. In this study we refer to the event as the post-Blake in light of the recent review by Singer (2014) on the Quaternary geomagnetic instability scale (GITS). The age of this excursion agrees well with the constraints provided by the dated tephra beds that bracket it.

Magnetic susceptibility was measured on the same samples

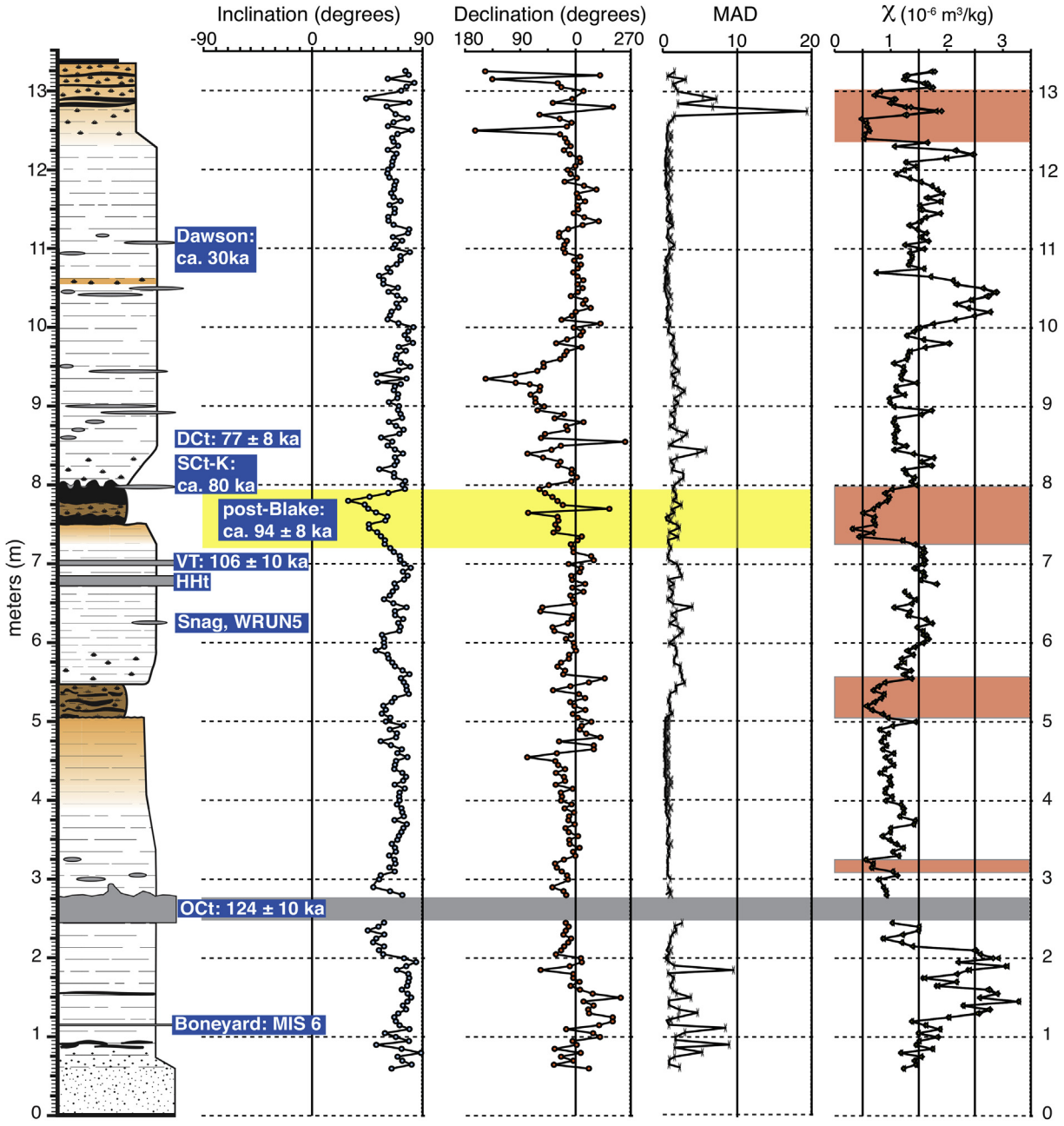

Fig. 11. Stratigraphic log of Halfway House including significant tephra beds, as well as inclination, declination, MAD, and magnetic susceptibility (χ) profiles. Highlighted in yellow is the post-Blake excursion. Lowest χ measurements are associated with paleosols and are highlighted. The exception is the small deviation above OCt, which is not associated with any morphologically distinct paleosol in trench 3 (this study, Muhs et al., 2003, 2008), but has been described by Lagroix et al. (2004a,b) in trench 1 at a similar level.

used to determine of inclination and declination data, resulting in a high-resolution profile that is virtually identical to that reported by Lagroix and Banerjee (2004a), Oches et al. (1998) and Vlag et al. (1999) from trench 1. This provides the opportunity to place previous research within the new chronologic framework (Figs. 3 and 13).

5. Discussion

5.1. Interpreting detrital tephra

Loess at Halfway House contains a background of detrital glass shards that complicate analyses of small samples. Two small (~1 mm wisps) samples collected near Boneyard tephra were comprised of glass shards that do not form any interpretable geochemical populations, and have no affinity to any of the tephra present at Halfway House. UA 1872, containing HH1 and HH2 as the most abundant populations, also contained 5 shards of HH3, which was later identified in virtually every sample collected above UA 1872. OCt and HHt are also frequently present as detrital shards in samples collected above their respective stratigraphic levels. Moving up the stratigraphic column, new populations appear, for example, DCt and DAB ~50 cm above SCt-K (Fig. 11). In the case of DCt in particular, its well-documented stratigraphic relationship with SCt-K from other locations adds confidence to the stratigraphy at Halfway House, despite the nature of the tephra samples that

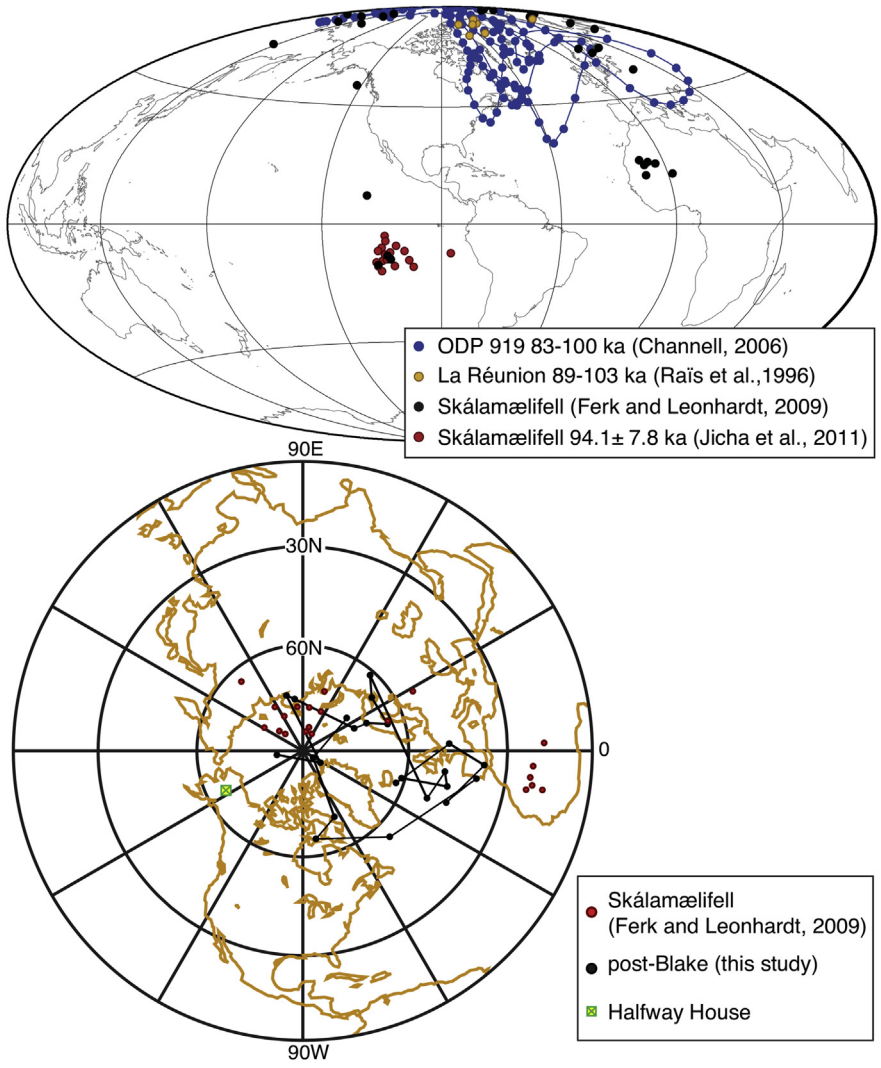

Fig. 12. Top: A series of VGP paths from the interval containing the post-Blake compared to those from the Skálamælifell lava flows (modified from Jicha et al., 2011). Bottom: Halfway House VPGs from samples collected between 6.95 and 8.10 m describe a path towards the North African VGPs of Ferk and Leonhardt (2009).

comprise it (Fig. 3). Therefore, it seems probable that the first appearance of shards in a sample correlating to a known tephra bed will provide an approximate maximum age for the loess at that stratigraphic level, and, at a minimum, all loess above this point must post-date the age of that tephra.

The presence of detrital glass from reworked tephra at the site suggests that some of the loess is derived from (locally?) re-entrained sediments. This supports Muhs et al.'s (2003) alternative hypothesis, that the loess has ^{10}Be inheritance due to previous subaerial exposure, to explain some of the problematic ^{10}Be ages at this site.

5.2. A chronologic framework for Halfway House

Prior to this research, only four tephra beds had been described at Halfway House: Boneyard, Old Crow, Halfway House and VT (Westgate et al., 1983, 1985; Preece et al., 1999; Jensen et al., 2013). Revised age determinations for OCt and VT have been presented in recent years, and the Boneyard tephra has a regionally consistent stratigraphic context that provides insight into its time of deposition.

The Boneyard tephra is within ~1 m of OCt at all sites where it has been identified, although it has not been found in direct stratigraphic context with Sheep Creek-Fairbanks (SCt-F), another tephra commonly associated with OCt that has a thermoluminescence age of 190 ± 20 ka (Berger et al., 1996; Preece et al., 1999; Westgate et al., 2008; Jensen et al., 2013). However, at the Palisades (reference site for the Boneyard tephra) and Eva Creek, two sites where SCt-F is in clear stratigraphic context with OCt, SCt-F is consistently found 3–6 m below OCt (Preece et al., 1999; Muhs et al., 2001; Jensen et al., 2013). This juxtaposition suggests that Boneyard tephra is bracketed by SCt-F and OCt, and was deposited during MIS 6.

The most recent recalculation of multiple fission-track ages for OCt places it roughly within MIS 5e (124 ± 10 ka,104–144 ka at two sigma range; Preece et al., 2011a). However, Reyes et al. (2010b) described a site at the Palisades where a primary bed of OCt buried a vegetated surface. The pollen, plant and insect fossils from this surface show tundra conditions still existed at the time of deposition. Further careful documentation of multiple sites around Alaska and the Yukon where the tephra occurs in association with MIS 5e deposits show that the tephra clearly predates MIS 5e (Reyes et al., 2010a). Thus, based on stratigraphic relations, and within error of revised the fission-track age estimate; we interpret

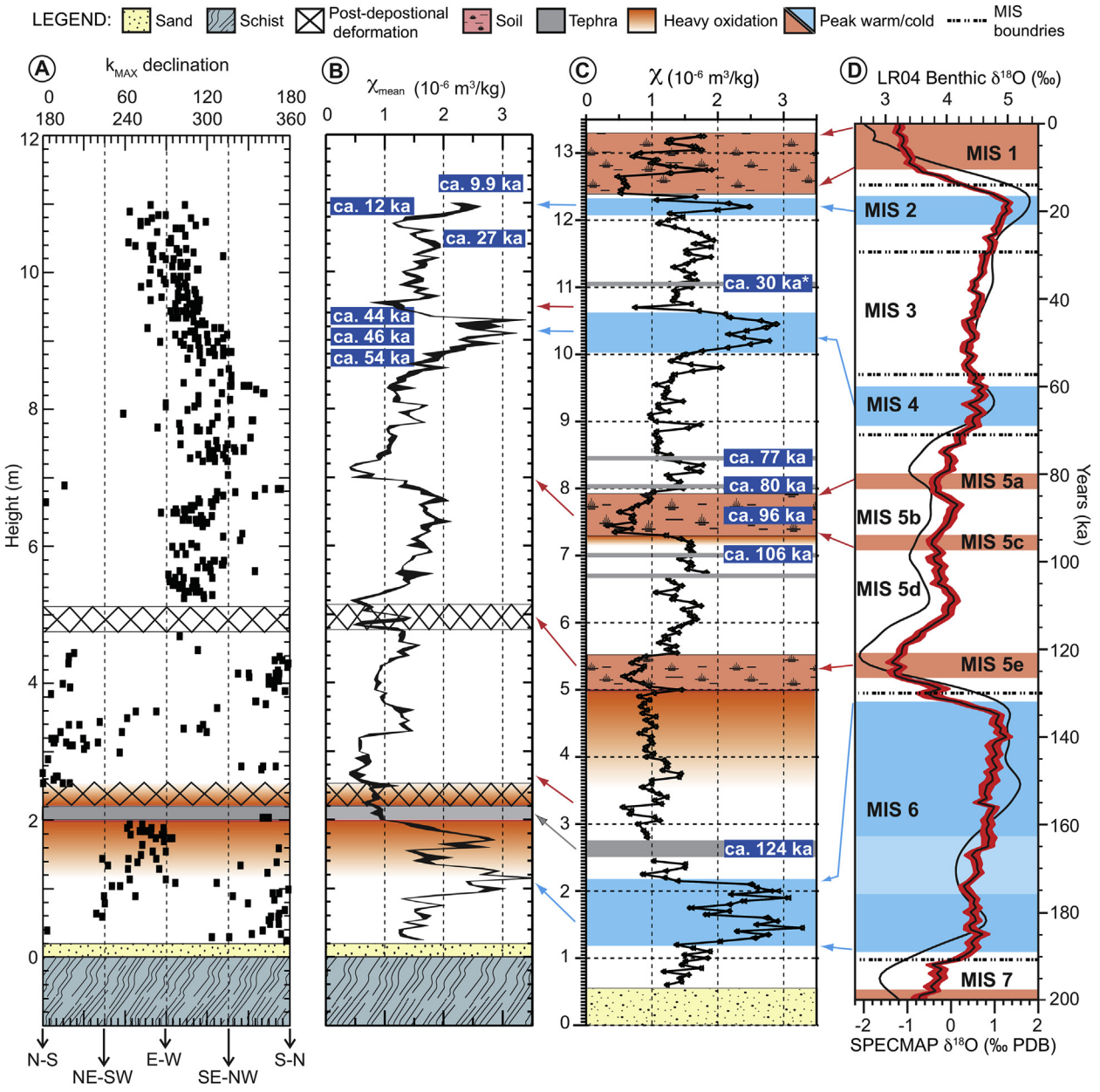

Fig. 13. Correlation of Lagroix and Banerjee (2004a) wind-direction (*A*) and susceptibility (*B*) profiles to the susceptibility and stratigraphic profile from this study (*C*), and the LR04 oxygen isotope stack (*D*) (Lisieski and Raymo, 2005). The SPECMAP profile (*D*; black curve) is included for comparison (Imbrie et al., 1984). MIS divisions are based on the LR05 record. k_{max} = maximum susceptibility axes; χ_{mean} of 5 samples collected at each 5-cm interval. Ages from dated tephra beds and the excursion are included on *(C)*, TL ages from Oches et al. (1998) that are considered the most reliable are included on *(B)*. *This age is from the Dawson tephra, but here represents the maximum age as the tephra is likely detrital.

the OCt to have been deposited some time in late MIS 6.

Age control on HHt is provided by VT tephra, which lies directly above HHt at Halfway House and Gold Hill, and by an MIS 5e forest bed that underlies it at the Palisades (Preece et al., 1999; Berger, 2003; Jensen et al., 2013). The new SAR-IRSL age for VT of 106 ± 10 ka is consistent with evidence at other sites where the tephra is found (Jensen et al., 2011). In particular, the correlation of the Aeolis Mountain tephra (Togiak Bay, SW Alaska; Kaufman et al., 2001) to VT, present in a coastal bluff with independent chronologic control and a high-resolution pollen profile, suggest VT was deposited during a stadial in MIS 5 that likely corresponds to MIS 5d (Kaufman et al., 2001; Jensen et al., 2011).

The correlation of the HH1 and HH2 to Snag tephra and WR-UN5 is supported by their close stratigraphic relationship to VT at Halfway House. Turner et al. (2013) report Snag tephra at a 5 km long bluff on the White River, southwestern Yukon. This bluff exposes a sequence of till, non-glacial deposits, and abundant tephra beds, including OCt, DCt and Dawson. Snag tephra is a newly described bed presented in this study, which is found stratigraphically above OCt and associated MIS 5e deposits, and below a woody peat unit representing MIS 5a that has DCt (77 ± 8 ka) overlying it. WR-UN5, although not reported in Turner et al. (2013), is present in close association with Snag at several exposures at this site (Turner, pers. comm.).

The identification of SCt-K, deposited directly on the surface of the paleosol couplet, and DCt shards first appearing in samples

~50 cm above SCt-K, supports a late MIS 5 age for the couplet. SCt-K is widely distributed in the Klondike area of central Yukon. Stratigraphically, SCt-K is consistently found directly above a forest bed, and generally ≤1 m below DCt, which has a glass fission-track age of 77 ± 8 ka (e.g. Sanborn et al., 2006; Westgate et al., 2008; Preece et al., 2011b; Zazula et al., 2011). OSL ages reported by Westgate et al. (2008) of ~80 ka are in agreement with the age of DCt. Together, these tephras date the forest bed below SCt-K to MIS 5a. Schweger (2003) reported a detailed, 9-m long, pollen profile through the Ash Bend site on the Stewart River, central Yukon, that shows the progression from boreal forest, to forest tundra, to birch tundra, to herb tundra. SCt-K is present ~1.5 m above the transition from boreal forest to forest tundra, and is firmly within the latter. This indicates that SCt-K was deposited relatively early in the transition from full interglacial conditions of MIS 5a (boreal forest) to full glacial conditions of MIS 4 (herb tundra). The replication of this well-documented stratigraphic relationship at Halfway House allows correlation to Ash Bend and revises the age of the paleosol couplet below these tephra beds from the early to mid-Wisconsinan to late MIS 5.

Whether the paleosol couplet is entirely attributable to MIS 5a or is a complex that represents MIS 5c, 5b and 5a is not clear. The post-Blake excursion is most accurately dated to 94.1 ± 7.8 ka in Iceland, and most strongly expressed in marine paleointensity records during MIS 5c (~100–95 ka) (Thouveny et al., 2004, 2008; Jicha et al., 2011). There is little evidence for an unconformity in this interval, and Lagroix and Banerjee (2004b) did not find evidence of post-depositional deformation (Fig. 13). The excursion begins ~15 cm below the lower A-horizon, consistent with the age control provided by VT, but continues through the couplet, with inclination values not recovering until ~10 cm below SCt-K. Finding SCt-K on the surface of the paleosol suggests that it is MIS 5a in age, but it seems improbable, despite the relatively lengthy duration of the paleointensity low, that the excursion lasted for >10 ka. What seems more likely is that the upper portion of the paleosol may have been partially removed during MIS 5a, or there was a hiatus in loess deposition during peak MIS 5a, resulting in soil formation on older loess.

The inevitable question that arises from the presence of the post-Blake event, is the absence of the Blake event. Although records of the timing and duration of the Blake event are variable, most studies place it between ca. 125–115 ka, making it largely coincident with MIS 5e (e.g. Singer and Hoffman, 2005; Lund et al., 2006; Channell et al., 2012; Singer, 2014). Inclination measurements at Halfway House reported by Westgate et al. (1983, 1985) found a shallowing below OCt, an event that has been reported in the same stratigraphic position in cores from Imuruk Lake on the Seward Peninsula and Koyukuk Bluff (KY11) in central Alaska (e.g. Schweger and Matthews, 1985). We were not able to reproduce these results at Halfway House. Although originally interpreted as representing the Blake event, this is unlikely because they are present below OCt (late MIS 6). However, recent identification of an excursion above OCt and directly below an *in situ* MIS 5e forest bed at the Palisades, central Alaska, suggests the Blake is recorded in Alaskan loess of the appropriate age when it has not been disturbed or removed by MIS 5 thaw (Jensen et al., 2013). At Halfway House, the paleosol from 5 to 5.5 m is interpreted to represent peak MIS 5e, and corresponds to one of two intervals where Lagroix and Banerjee (2004b) found evidence of post-depositional deformation (Fig. 13). Muhs et al. (2008) also suggested that this paleosol may have experienced some erosion, partially truncating the top of the pedogenic geochemical profile. Thus, the absence of the Blake at Halfway House may be a result of the disturbance and/or absence of the loess in which the event would have been recorded.

The next dated point in the stratigraphic column is at ~11 m with the correlation of HH8 to the Dawson tephra. This tephra is found extensively throughout the Klondike goldfields (e.g. Westgate et al., 2000; Froese et al., 2002, 2006). Two grass leaves collected from an *in situ* surface buried by this tephra at the Goldbottom site in the Klondike are dated to 25,410 ± 160 and 25,210 ± 260 ^{14}C yr BP (Froese et al., 2006). Further Bayesian analysis of these ages and five additional radiocarbon dates estimate the time of deposition for Dawson between 30,433 and 30,032 cal yr BP (Demuro et al., 2008). Dawson tephra is found above organic-rich deposits that are MIS 3 in age, but plant macrofossil data directly associated with the tephra suggests that the environment of MIS 2 (i.e. steppe-tundra) is established by the time of deposition (Zazula et al., 2005, 2007; Froese et al., 2006). Because the population of Dawson tephra in HH8 is likely detrital, and no samples were collected below this level in trench 1, it is not certain if HH8 represents the first occurrence of Dawson at Halfway House. Some insight into this problem is provided by the correlation of UA 1908 from Gold Hill III (for location details see Evans et al., 2011) to Dawson tephra (Fig. 8). UA 1908 was collected laterally from, and ~75 cm below, UA 1907. UA 1907 correlates to HH7 and at Gold Hill III is a discrete, mm-scale, continuous bed. Therefore, it appears that Dawson tephra predates HH7, which was collected at the same stratigraphic level at Halfway House.

HH7 has been correlated to Eva Creek, Gold Hill III and IV, and the Engineering Creek/Dawson Cut locales in this study, and at all sites it is 1–3 m below the surface within massive inorganic loess. HH7 potentially correlates to the Chatanika and/or EB tephras, although the possibility that all could be unique units cannot be discounted. The stratigraphic context of each tephra does not clarify this problem, as they are all similar to one another. EB tephra was collected at the Eva Bench cut, adjacent to the more widely studied Eva Creek exposure, in what was thought to be the base of the Holocene Engineer Loess, although there are no independent ages to confirm this assumption (Péwé et al., 2009). Chatanika tephra was similarly located in inorganic loess considered late Pleistocene in age. At its reference locality along the Chatanika River, Péwé (1975b) reports radiocarbon ages (1 sigma error) bracketing the Chatanika tephra: a date of 14,760 ± 850 ^{14}C yr BP from a ground squirrel nest ~2 m below the tephra, and a second date of 14,510 ± 450 ^{14}C yr on coprolites extracted from another nest ~1.5 m above the tephra.

5.3. Magnetic susceptibility at Halfway House

As reviewed previously, wind intensity is the main variable that controls changes in magnetic susceptibility in regions such as Alaska and Siberia: ferromagnetic grains are more abundant and larger in loess during times of higher wind-intensity (i.e. glacials), than during times of lower wind-intensity (i.e. interglacials) (e.g. Begét and Hawkins, 1989; Begét et al., 1990; Vlag et al., 1999).

Consistent with previous studies, we find the lowest values in the magnetic susceptibility at Halfway House are present in the modern soil complex, the late MIS 5c–5a paleosol complex, and the MIS 5e paleosol. Additional short-lived susceptibility lows are present above OCt (~3.25 m) and at ~10.6 m; though both are better expressed in Lagroix and Banerjee's (2004a) profile of trench 1 (Fig. 13). The low at ~10.6 m is below the Dawson tephra (ca. 30 ka), and thus may be associated with a very poorly expressed paleosol of MIS 3 age; paleosols of this age have been documented at several sites around Fairbanks (e.g. Hamilton et al., 1988; Muhs et al., 2003, 2008).

The persistent, relatively low values below the MIS 5e paleosol to ~30 cm above OCt raises the possibility that MIS 5e is represented by that entire interval (Fig. 13). However, although Muhs et al. (2003, 2008) geochemically identify a truncated soil around

the level corresponding to the lowest susceptibility values at ~3.25 m, there is no evidence, morphologically or geochemically, for other individual paleosols through this interval. This interval is also comprised of the heavily oxidized, friable loess with clay lamellae described in this study; Muhs et al. (2008) show that measured ratios of mobile to immobile elements, an indication of the degree of weathering, is lowest in the paleosol at ~5 m and remains notably low throughout this section (Fig. 4). This raises the possibility that this interval may be a B-horizon related to the MIS 5e paleosol at ~5 m, and that weathering could have played a role in lowering susceptibility in this interval. Weathering, particularly when related to poorly drained conditions, can lead to some loss of magnetic grains within Alaskan loess (Lui et al., 1999, 2001; Begét, 2001). An alternative explanation is revealed by the wind-direction data reported by Lagroix and Banerjee (2004a); this interval is the only major interval that shows a change in wind direction (Fig. 13). If this is the case, the steady low in susceptibility could reflect a changing source, particularly if that source is more distal. In support of this interpretation, this is the only interval where Muhs et al. (2008) document a change in the geochemistry of the loess at Halfway House that they interpret as being driven by an influx of loess derived from the Nenana River, a more distant source than the Tanana River (Fig. 4).

The slight variation in geochemistry that is tentatively identified as a truncated paleosol by Muhs et al. (2003, 2008) appears to correspond to the susceptibility low at ~3.25 m, which was correlated to MIS 5e by Lagroix and Banerjee (2004a). This correlation does not appear likely, but it is a notable feature in the profile, and its presence in latest MIS 6 suggests it could be related to the Zeifen-Kattegat climate oscillation (Seidenkrantz et al., 1996). There is evidence of "two-step" deglaciation at the termination of MIS 6 that is considered analogous to the Younger Dryas, where warming at the termination of MIS 2 was interrupted by an abrupt return to glacial conditions before resuming the transition to interglacial conditions (e.g. Seidenkrantz et al., 1996). The Zeifen-Kattegat climate oscillation is documented in pollen records across Yukon and Alaska; at Imuruk Lake, Koyukuk Bluff, Chi'jees Bluff and Birch Creek, where spruce pollen appears for a short interval directly above OCt, but is then absent again until MIS 5e (e.g. Seidenkrantz et al., 1996; McDowell and Edwards, 2001; Reyes et al., 2010b).

The highest susceptibility values are found below OCt (~1–2 m), below Dawson tephra (~10–10.5 m), and above Dawson tephra (~12.25 m) (Fig. 13). Age control provided by the tephra beds implies that these highs correspond to MIS 6, 4 and 2, respectively. MIS 6 and 4 are better expressed than MIS 2, and this pattern is also present in the susceptibility record for the upper ~8 m of Gold Hill IV. The chronology for this latter correlation is provided via the VT and HH7 tephra beds (Fig. 15). Although MIS 6 is absent at Gold Hill IV (a large unconformity underlies VT related to thaw during MIS 5e), the record indicates that MIS 4 is more strongly represented than MIS 2.

The most striking feature of the overall magnetic susceptibility profile is how it is predominantly comprised of intermediate values. This suggests that the majority of accumulation at Halfway House corresponds to times of moderate wind intensity, which would likely correspond to stadials, interstadials or transitions between MIS stages, an assumption supported by the chronology. These results force the modification of existing loess accumulation models in Alaska.

5.4. Loess accumulation in interior Alaska

Silt in Alaska is produced by glacial comminution, without glaciers there would be little, if any, loess accumulation. However, the proximity of interior Alaska to glaciers, both presently and in the past, also complicates attempts to understand loess accumulation in the region. This complexity is highlighted by Muhs' et al. (2003) model for loess accumulation that argues that while production is greatest during full glacial conditions, accumulation rates during these times are relatively low. They suggest that this reversal reflects the role of surface roughness. For example, while loess production during full glacial conditions was high, the landscape was largely covered by herb or steppe-tundra with a low profile and limited capacity to capture and hold sediment. In contrast, during interglacials boreal forest is present, with high surface roughness, leading to higher rates of accumulation despite lower rates of production (e.g. Muhs et al., 2004). During interstadials, production is considered high, but accumulation only moderate (Fig. 15).

Our magnetic susceptibility profile, placed in the new chronology, allows us to test this model. Peak values of susceptibility, linked to wind intensity and full glacial conditions are not the dominant feature of the profile. However, while there is very little accumulation during MIS 2, consistent with the full glacial scenario of Muhs' et al. (2003, 2004) model and their observations from several equivalent-aged loess localities around Fairbanks, we do find that there is accumulation during MIS 4 and 6. The minimal amount of loess from MIS 2 is consistent with glacial records in Alaska that indicate MIS 4 and MIS 6 ice limits, from both the Alaska and Brooks Ranges, were more extensive than during MIS 2 (e.g. Briner and Kaufman, 2008; Dortch et al., 2010; Matmon et al., 2010). This suggests while surface roughness may be the

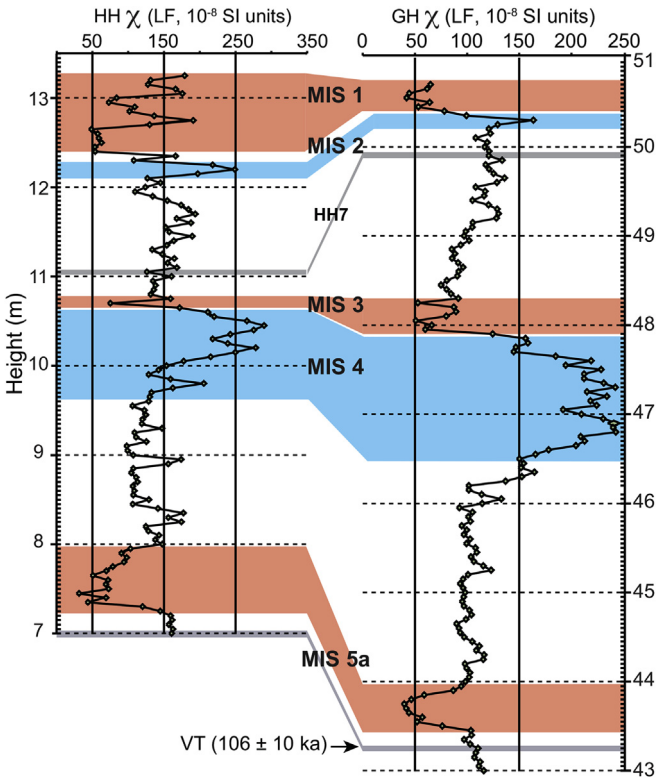

Fig. 14. Correlation of the Halfway House and Gold Hill IV susceptibility profiles. The correlation is supported by the presence of VT (106 ± 10 ka) and HH7 at both sites. Dawson tephra (ca. 30 cal yr BP) is not present at Gold Hill IV, but is ~50 cm below HH7 at Gold Hill III, approximately 150 m southwest from Gold Hill IV. Neither DCt (77 ± 8 ka) or SCt-K (ca. 80 ka) have been found at Gold Hill, but DAB is present at the Gold Hill Steps section, ~200 m east on the George Parks Highway. This suggests that the prominent humified peat unit that is ubiquitous several meters below the surface across much of Gold Hill is most likely associated with MIS 3, consistent with radiocarbon dates, but the paleosol below DAB at Gold Hill Steps is likely associated with MIS 5a rather than an early to mid-Wisconsinan interstadial (e.g. Muhs et al., 2003).

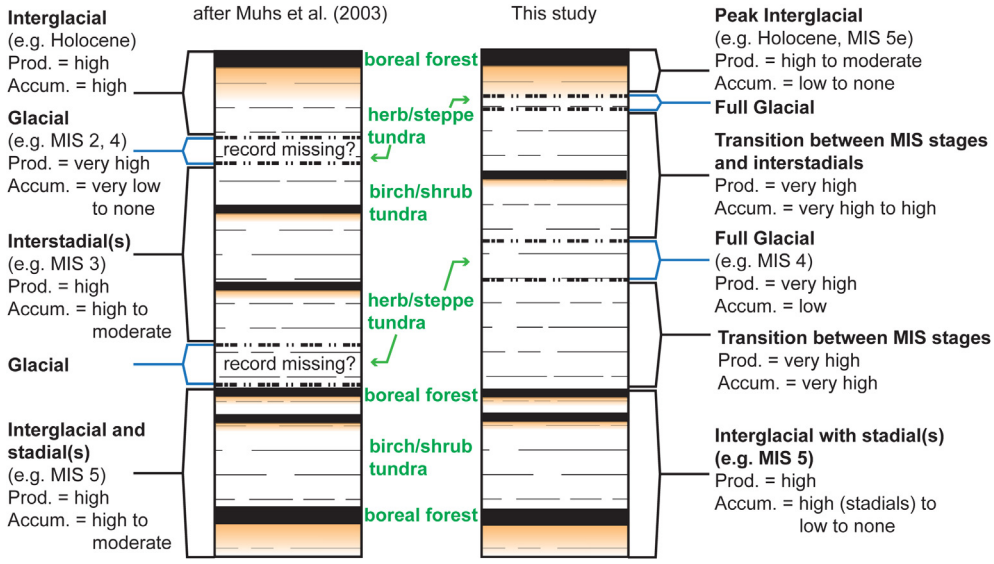

Fig. 15. Comparison of Muhs et al. (2003) idealized loess accumulation model, roughly based on Halfway House stratigraphy, to the one developed in this study using magnetic susceptibility and new age data as guides. The models are similar but peak susceptibility measurements indicate full glacial loess is present, there may be a hiatus during peak interglacial warmth, and that more loess appears to accumulate during transitions between isotope stages than at any other time.

controlling variable during full glacials, the production of silt is still important.

We also do not see significant loess accumulation during periods of peak warmth in MIS 5, and, in fact, a hiatus may even be present. It follows that during peak interglacial warmth, although surface roughness is high, glaciers are at their minimum extent and silt production is low, and thus becomes more critical than surface roughness as the dominant variable controlling accumulation rates.

As noted previously, most of the loess has intermediate susceptibility values, reflecting moderate wind conditions (and potentially distance from source). These conditions and the new chronology suggest that the highest rates of accumulation at Halfway House and the upper-most portion of Gold Hill occur during transitions between isotope stages, and to a lesser extent, stadials and interstadials. With glaciers advancing or retreating at these times, production rates would have been relatively high, as well as surface roughness, since transitional environments would have consisted more of shrub tundra, potentially interspersed with stands of trees such as birch and aspen, and even sparse spruce (e.g. Anderson and Lozhkin, 2001; Brubaker et al., 2001, 2005; Schweger, 2003). This represents optimal conditions for loess accumulation, where loess production and surface roughness are both relatively high.

There are factors that should be considered when applying this revised model:

(1) It is most applicable to the thicker loess deposits that are found more “distally” from their glacial sources. For example, loess deposits closer to source (e.g. in the Matanuska, Tanana, Delta or Nenana river valleys 10 s of kms from or in the Alaska Range, near present or past glacial limits) tend to preserve shorter records and may, in fact, only preserve interglacial loess. This may be the result of ice covering the area during an advance, or the high wind intensity and low height of the vegetative surface during glacials resulting in deflation (e.g. Thorson and Bender, 1985; Begét, 2001; Muhs et al., 2004).

(2) Many loess deposits fill topographic lows (i.e. valleys) or are on the lee-side of bedrock highs. For example, the conspicuously thick Gold Hill loess is deposited over a particularly low bedrock hill (e.g. Pewe et al., 2009). However, once the deposit reaches the elevation of the local surface (filling all available accommodation space), further deposition is unlikely and deflation may even occur. For example, the upper 8 m of late Pleistocene to Holocene loess at the top of Gold Hill IV is likely partially due to the lowering of the local surface by the MIS 5e thaw unconformity (Eva Creek Formation). This 8 m represents only ~100,000 years in a deposit that spans about 3 million years (e.g. Westgate et al., 1990). Therefore the upper 8 m of the section only covers 3% of the time represented, but makes up 13% of the section. This illustrates how changes in accommodation space can also enhance or minimize the deposition of loess in this region.

During MIS 5 there are likely short hiatuses in deposition and/or partial removal of paleosols (e.g. the decapitation of the MIS 5e paleosol) at Halfway House. Muhs et al. (2003) report ^{10}Be accumulation data that indicated the presence of an unconformity. They suggested that it was most likely located near OCt, which is not likely given the revised chronology, but doesn't preclude an unconformity higher in the section. However, although there appears to be a slow-down in accumulation in the upper ~1.5 m of the section, and the MIS 3 paleosol is not as well expressed as it is at Gold Hill (possibly partially truncated); there is little evidence of a major unconformity. Overall, the chronology and magnetic susceptibility data presented here shows that Halfway House is somewhat unusual in comparison to many other loess exposures in this region in that it appears to be relatively continuous (e.g. Jensen et al., 2008; Péwé et al., 2009). While there is a no evidence for any prominent unconformities, the lateral continuity of the site cannot be fully examined, and it should be noted that the Holocene soil is not present in trench 2, although that may be the result of disturbance during the construction of the original road cut. Regardless, the relative continuity of the section and evidence for loess accumulation in the Holocene suggests that rates of loess deposition and changes in magnetic susceptibility at this site are more reflective of broad environmental and climatic changes rather than

variations in local conditions. If so, this site represents an ideal location to guide interpretations of other loess deposits in the region.

5.5. Marine isotope stage 5 in Alaska

In the Yukon there are multiple sites that preserve MIS 5a and 5e deposits, although only two sites are known with both in sequence (e.g. Westgate et al., 2008; Reyes et al., 2010a; Turner et al., 2013). At these sites, if other MIS 5 sediments are present, it is usually a loess unit containing one or more of series of tephra beds, such as Snag, Woodchopper Creek or Donjek, that identify it as MIS 5d (e.g. Turner, 2013). However, no evidence has been found of sediments that might have been deposited during MIS 5c or 5b.

Last interglacial deposits beyond MIS 5e are not clearly recognized in Alaska, but this could be the result of unreliable chronologies. For example, the Gold Hill Steps section, which has been examined along with Halfway House (e.g. Vlag et al., 1999; Muhs et al., 2003, 2008; Lagroix and Banerjee, 2004a,b), contains a similar susceptibility record and comparable stratigraphy in its upper ~8 m. Below a paleosol complex dated by Muhs et al. (2003, 2008) to the mid-Wisconsin (MIS 3), there is a peak in susceptibility that appears to correlate to the MIS 4 peak at Halfway House. Below this peak there is ~2.5 m of loess with intermediate susceptibility values to a well-developed paleosol, which is overlain by DAB. The correlation of Gold Hill Steps to Halfway House is supported by the correlation of Halfway House to the upper 8 m of the Gold Hill IV exposure (GHIV; Fig. 14), which is only ~200 m from the steps. The stratigraphic and magnetic susceptibility records between the upper 8 m of GHIV and Gold Hill Steps are virtually indistinguishable, except for the absence of DAB at GHIV (Vlag et al., 1999, Fig. 14). Muhs et al. (2008) suggest the paleosol below DAB at Gold Hill Steps is representative of the last interglacial, however, in light of the evidence at Halfway House and Gold Hill IV, it seems more likely that it was formed during MIS 5a. Probable MIS 4 deposits and DAB were also identified at Eva Creek (Muhs et al., 2001). Therefore, MIS 5 sediments, in addition to MIS 5e, may be more common in Alaska than has previously considered.

6. Conclusions

The Halfway House site is one of the most studied loess sections in Alaska, but interpretations of those studies have been limited by poor chronological control. Systematic re-examination of the tephrostratigraphy has identified several dated tephra beds not previously recognized at the site: SCt-K (ca. 80 ka), DCt (77 ± 8 ka) and Dawson (~30 cal yr BP). The presence of the post-Blake excursion (94.1 ± 7.8 ka) provides an independent age at the site, and supports the chronology provided by SCt-K and VT (106 ± 10 ka), which bracket the excursion. These ages, and the presence of Old Crow (124 ± 10 ka) and Boneyard tephras, indicate that Halfway House has a relatively complete MIS 6 to Holocene record, with little evidence of major unconformities, although there may be minor truncations and hiatuses, particularly through MIS 5. This revised chronology also indicates the presence of two major paleosols that formed during MIS 5 (Fig. 13). The identification of Snag, WR-UN5, SCt-K, and DCt is the first documentation of these tephra beds outside of the Yukon, and indicates that they are important regional markers for MIS 5d (Snag, WR-UN5) and MIS 5a (SCt-K, DCt). The appearance of DAB glass shards above the late MIS 5 paleosol at Halfway House, and the implication that the paleosol below DAB at the Gold Hill Steps site correlates to this paleosol, suggests that this tephra bed is of similar age to DCt (ca. 77 ka), and that MIS 5a may be more represented in Alaska than previously considered.

These new ages, when placed on the magnetic susceptibility profile, show that loess accumulation at Halfway House is highest during transitions between MIS stages, interstadials and stadials, with low loess accumulation during peak cold and peak warm intervals. This is partially consistent with the loess accumulation model presented by Muhs et al. (2003), where loess production and accumulation are not positively correlated, and surface roughness is the leading variable controlling accumulation rates. In contrast to their model, we find that during full glacial conditions there is evidence for some accumulation (albeit generally at lower rates), but also find a lack of evidence for high accumulation rates during peak interglacial times. We modify the model to suggest that loess production is the most important variable controlling accumulation during times of extensive glacier retreat (e.g. MIS 5e), and that the greatest amount of accumulation is during times when loess production, surface roughness, and wind intensity are all relatively moderate.

The complexity of highly variable accumulation rates dependent on the interplay of wind intensity, loess production, surface roughness and location of the site, demands the development of robust chronologies when attempting to link Alaskan magnetic susceptibility profiles to global $\delta^{18}O$ curves or other paleoclimate and paleomagnetic records. However, once the chronology is established, the almost ideal paleomagnetic characteristics of these loess deposits shows that they are exceptional archives that provide important insights into past regional and global paleomagnetic and paleoenvironmental variations.

Acknowledgments

This research was funded by the Natural Sciences and Engineering Research Council of Canada (D.G.F.), and grants from the Canadian Circumpolar Institute and Northern Scientific Training Program (B.J.L.J.). B.J.L.J. acknowledges scholarship support from NSERC, Alberta Ingenuity, and the Killam Trusts. Excellent assistance with the hard labour and patience required for the fieldwork were provided by H. Dunning and J. Pumple. We thank F. Lagroix for generously providing access to figures and photos on her research at Halfway House that helped us properly pinpoint the sections referred to in previous research, and S.J. Preece and J.A. Westgate for providing reference material for EB, Chatanika, Dominion Creek and DAB tephra beds. B.J.L.J. also thanks Dr. Anders Carlson for providing the space and time to complete her PhD while a visiting scientist at the University of Wisconsin-Madison, where the first iteration of this study appears. We also thank the reviewers, France Lagroix and Dan Muhs for their constructive comments that resulted in an improved manuscript.

Appendix A. Supplementary data

Supplementary data related to this article can be found at http://dx.doi.org/10.1016/j.quascirev.2016.01.001.

References

Anderson, P.M., Lozhkin, A.V., 2001. The stage 3 interstadial complex (Karginskii/middle Wisconsinan interval) of Beringia: variations in paleoenvironments and implications for paleoclimatic interpretations. Quat. Sci. Rev. 20, 93–125.
Auclair, M., Lamothe, M., Lagroix, F., Banerjee, S., 2007. Luminescence investigation of loess and tephra from Halfway House section, Central Alaska. Quat. Geochronol. 2, 34–38.
Begét, J., 1990. Middle Wisconsinan climate fluctuations recorded in central Alaskan loess. Géogr. Physique Quaternaire 44, 3–13.
Begét, J., 1996. Tephrochronology and paleoclimatology of the last interglacial-glacial cycle recorded in Alaskan loess deposits. Quat. Int. 34, 121–126.
Begét, J.E., 2001. Continuous Late Quaternary proxy climate records from loess in Beringia. Quat. Sci. Rev. 20, 499–507.
Begét, J.E., Hawkins, D.B., 1989. Influence of orbital parameters on Pleistocene loess

deposition in central Alaska. Nature 337, 151–153.
Begét, J.E., Keskinen, M., 1991. The Stampede tephra: a middle Pleistocene marker bed in glacial and eolian deposits of central Alaska. Can. J. Earth Sci. 287, 991–1002.
Begét, J.E., Stone, D.B., Hawkins, D.B., 1990. Paleoclimatic forcing of magnetic susceptibility variations in Alaskan loess during the late Quaternary. Geology 18, 40–43.
Berger, G.W., Péwé, T.L., Westgate, J.A., Preece, S.J., 1996. Age of Sheep Creek tephra (Pleistocene) in central Alaska from thermoluminescence dating of bracketing loess. Quat. Res. 45, 263–270. http://dx.doi.org/10.1006/qres.1996.0027.
Berger, G.W., 2003. Luminescence chronology of late Pleistocene loess-paleosol and tephra sequences near Fairbanks, Alaska. Quat. Res. 60, 70–83. http://dx.doi.org/10.1016/S0033-5894(03)00060-7.
Briner, J.P., Kaufman, D.S., 2008. Late Pleistocene mountain glaciation in Alaska: key chronologies. J. Quat. Sci. 23, 659–670. http://dx.doi.org/10.1002/jqs.1196.
Brubaker, L.B., Anderson, P.M., Hu, F.S., 2001. Vegetation ecotone dynamics in Southwest Alaska during the Late Quaternary. Quat. Sci. Rev. 20, 175–188.
Brubaker, L.B., Anderson, P.M., Edwards, M.E., Lozhkin, A., 2005. Beringia as a glacial refugium for boreal trees and shrubs: new perspectives from mapped pollen data. J. Biogeogr. 32, 833–848. http://dx.doi.org/10.1111/j.1365-2699.2004.01203.x.
Carcaillet, J., Bourlès, D.L., Thouveny, N., Arnold, M., 2004. A high resolution authigenic $^{10}Be/^{9}Be$ record of geomagnetic moment variations over the last 300 ka from sedimentary cores of the Portuguese margin. Earth Planet. Sci. Lett. 219, 397–412. http://dx.doi.org/10.1016/S0012-821X(03)00702-7.
Channell, J.E.T., Xuan, C., Hodell, D.A., 2009. Stacking paleointensity and oxygen isotope data for the last 1.5 Myr (PISO-1500). Earth Planet. Sci. Lett. 283, 14–23. http://dx.doi.org/10.1016/j.epsl.2009.03.012.
Channell, J.E.T., Hodell, D.A., Curtis, J.H., 2012. ODP Site 1063 (Bermuda Rise) revisited: oxygen isotopes, excursions and paleointensity in the Brunhes Chron. Geochem. Geophys. Geosyst. 13 http://dx.doi.org/10.1029/2011GC003897. Q02001.
Chlachula, J., Evans, M.E., Rutter, N.W., 1998. A magnetic investigation of a late Quaternary loess/palaeosol record in Siberia. Geophys. J. Int. 132, 128–132.
Demuro, M., Roberts, R.G., Froese, D.G., Arnold, L.J., Brock, F., Ramsey, C.B., 2008. Optically stimulated luminescence dating of single and multiple grains of quartz from perennially frozen loess in western Yukon Territory, Canada: comparison with radiocarbon chronologies for the late Pleistocene Dawson tephra. Quat. Geochronol. 3, 346–364. http://dx.doi.org/10.1016/j.quageo.2007.12.003.
Demuro, M., Arnold, L.J., Froese, D.G., Roberts, R.G., 2013. OSL dating of loess deposits bracketing Sheep Creek tephra beds, northwest Canada: Dim and problematic single-grain OSL characteristics and their effect on multi-grain age estimates. Quat. Gechronol. 15, 67–87. http://dx.doi.org/10.1016/j.quageo.2012.11.003.
Dortch, J.M., Owen, L.A., Caffee, M.W., Li, D., Lowell, T.V., 2010. Beryllium-10 surface exposure dating of glacial successions in the Central Alaska Range. J. Quat. Sci. 25, 1259–1269. http://dx.doi.org/10.1002/jqs.1406.
Enkin, R., Wuolle, K., McCann, C., Carretero, M., Voroney, M., Baylis, T., Morton, K., Jaycock, D., Baker, J., Beran, L., 2000. PMGSC, Paleomagnetism Data Analysis. Version 4.2. www.pgc.nrcan.gc.ca/tectonic/enkin.htm.
Evans, M.E., Rutter, N.W., Catto, N., Chlachula, J., Nyvlt, D., 2003. Magneto-climatology: teleconnection between the Siberian loess record and North Atlantic Heinrich events. Geology 31, 537–540.
Evans, M.E., Jensen, B.J.L., Kravchinsky, V.A., Froese, D.G., 2011. The Kamikatsura event in the gold Hill loess, Alaska. Geophys. Res. Lett. 38 http://dx.doi.org/10.1029/2011GL047793. L13302.
Ferk, A., Leonhardt, R., 2009. The Laschamp geomagnetic field excursion recorded in Icelandic lavas. Phys. Earth Planet. Inter. 177, 19–30. http://dx.doi.org/10.1016/j.pepi.2009.07.011.
Frank, M., Schwarz, B., Baumann, S., Kubik, P.W., Suter, M., Mangini, A., 1997. A 200 kyr record of cosmogenic radionuclide production rate and geomagnetic field intensity from ^{10}Be in globally stacked deep-sea sediments. Earth Planet. Sci. Lett. 149, 121–129.
Froese, D., Westgate, J., Preece, S., Storer, J., 2002. Age and significance of the late Pleistocene Dawson tephra in eastern Beringia. Quat. Sci. Rev. 21, 2137–2142.
Froese, D.G., Smith, D.G., Westgate, J.A., Ager, T.A., Preece, S.J., Sandhu, A., Enkin, R.J., Weber, F., 2003. Recurring middle Pleistocene outburst floods in east-central Alaska. Quat. Res. 60, 50–62. http://dx.doi.org/10.1016/S0033-5894(03)00090-5.
Froese, D.G., Zazula, G.D., Reyes, A.V., 2006. Seasonality of the late Pleistocene Dawson tephra and exceptional preservation of a buried riparian surface in central Yukon Territory, Canada. Quat. Sci. Rev. 25, 1542–1551. http://dx.doi.org/10.1016/j.quascirev.2006.01.028.
Froese, D.G., Zazula, G.D., Westgate, J.A., Preece, S.J., Sanborn, P.T., Reyes, A.V., Pearce, N.J.G., 2009. The Klondike goldfields and Pleistocene environments of Beringia. GSA Today 19, 4. http://dx.doi.org/10.1130/GSATG54A.1.
Gilmore, C.W., 1908. Smithsonian exploration in Alaska in 1907 in search of Pleistocene fossil vertebrates. Smithson. Misc. Collect. 51, 38.
Guthrie, R.D., 1968. Paleoecology of the large-mammal community in interior Alaska. Am. Midl. Nat. 79, 346–363. http://dx.doi.org/10.2307/2423182.
Guthrie, R.D., 1990. Frozen Fauna of the Mammoth Steppe: the Story of Blue Babe. University of Chicago Press, Chicago, p. 323.
Guyodo, Y., Valet, J.P., 1999. Global changes in intensity of the earth's magnetic field during the past 800 kyr. Nature 399, 249–252.
Hamilton, T.D., Craig, J.L., Sellman, P.V., 1988. The Fox permafrost tunnel: a late Quaternary geologic record in central Alaska. Geol. Soc. Am. Bull. 100, 948–969.
Heider, F., Zitzelsberger, A., Fabian, K., 1996. Magnetic susceptibility and remanent coercive force in grown magnetite crystals from 0.1 μm to 6 mm. Phys. Earth Planet. Inter. 93, 239–256.
Heller, F., Lui, T., 1986. Palaeoclimatic and sedimentary history from magnetic susceptibility of loess in China. Geophys. Res. Lett. 13, 1169–1172.
Imbrie, J., Hays, J.D., Martinson, D.G., McIntyre, A., Mix, A.C., Morley, J.J., Pisias, N.G., Prell, W.L., Shackleton, N.J., 1984. The orbital theory of Pleistocene climate: support from a revised chronology of the marine $\delta^{18}O$ record. In: Berger, A.L. (Ed.), Milankovitch and Climate, vol. 1D. Reidel Publishing Company, Norwell, MA, pp. 269–305.
Jensen, B., Froese, D., Preece, S., Westgate, J., Stachel, T., 2008. An extensive middle to late Pleistocene tephrochronologic record from east-central Alaska. Quat. Sci. Rev. 27, 411–427. http://dx.doi.org/10.1016/j.quascirev.2007.10.010.
Jensen, B.J.L., Preece, S.J., Lamothe, M., Pearce, N.J.G., Froese, D.G., Westgate, J.A., Schaefer, J., Begét, J., 2011. The Variegated (VT) tephra: a new regional marker for middle to late marine isotope stage 5 across Yukon and Alaska. Quat. Int. 246, 312–323. http://dx.doi.org/10.1016/j.quaint.2011.06.028.
Jensen, B.J.L., Reyes, A.V., Froese, D.G., Stone, D.B., 2013. The Palisades is a key reference site for the middle Pleistocene of eastern Beringia: new evidence from paleomagnetics and regional tephrostratigraphy. Quat. Sci. Rev. 63, 91–108. http://dx.doi.org/10.1016/j.quascirev.2012.11.035.
Jicha, B.R., Kristjánsson, L., Brown, M.C., Singer, B.S., Beard, B.L., Johnson, C.M., 2011. New age for the Skámælifell excursion and identification of a global geomagnetic even in the late Brunhes chron. Earth Planet. Sci. Lett. 310, 509–517. http://dx.doi.org/10.1016/j.epsl.2011.08.007.
Kaufman, D., Manley, W., Wolfe, A., Hu, F., Preece, S., Westgate, J., Forman, S., 2001. The last interglacial to glacial transition, Togiak Bay, southwestern Alaska. Quat. Res. 55, 190–202.
Kravchinsky, V.A., Zykina, V.S., Zykin, V.S., 2008. Magnetic indicator of global paleoclimate cycles in Siberian loess. Earth Planet. Sci. Lett. 265, 498–514. http://dx.doi.org/10.1016/j.epsl.2007.10.031.
Kristjánsson, L., Gudmundsson, A., 1980. Geomagnetic excursion in late-glacial basalt outcrops in south-western Iceland. Geophys. Res. Lett. 7, 337–340.
Kristjánsson, L., 2003. Paleomagnetic observations on Late Quaternary basalts around Reykjavík and on the Reykjanes peninsula, SW-Iceland. Jökull 52, 21–32.
Kukla, G., 1987. Loess stratigraphy in central China. Quat. Sci. Rev. 6, 191–219.
Kukla, G., Heller, F., Ming, L.X., Chun, X.T., Sheng, L.T., Sheng, A.Z., 1988. Pleistocene climates in China dated by magnetic susceptibility. Geology 16, 811–814.
Lagroix, F., Banerjee, S.K., 2002. Paleowind directions from the magnetic fabric of loess profiles in central Alaska. Earth Planet. Sci. Lett. 195, 99–112. http://dx.doi.org/10.1016/S0012-821X(01)00564-7.
Lagroix, F., Banerjee, S.K., 2004a. The regional and temporal significance of primary aeolian magnetic fabrics preserved in Alaskan loess. Earth Planet. Sci. Lett. 225, 379–395. http://dx.doi.org/10.1016/j.epsl.2004.07.003.
Lagroix, F., Banerjee, S.K., 2004b. Cryptic post-depositional reworking in aeolian sediments revealed by the anisotropy of magnetic susceptibility. Earth Planet. Sci. Lett. 224, 453–459. http://dx.doi.org/10.1016/j.epsl.2004.05.029.
Lagroix, F., Banerjee, S.K., Jackson, M.J., 2004. Magnetic properties of the Old Crow tephra: identification of a complex iron titanium oxide mineralogy. J. Geophys. Res. 109 http://dx.doi.org/10.1029/2003JB002678. B01104.
Levi, S., Audunsson, H., Duncan, R.A., Kristjánsson, L., Gillot, P.Y., Jakobsson, S.P., 1990. Late Pleistocene geomagnetic excursion in Icelandic lavas: confirmation of the Laschamp excursion. Earth Planet. Sci. Lett. 96, 443–457.
Lisiecki, L.E., Raymo, M.E., 2005. A Pliocene–Pleistocene stack of 57 globally distributed benthic $\delta^{18}O$ records. Paleoceanography 20, 522–533.
Liu, T., Zhang, S., Han, J., 1986. Stratigraphy and paleoenvironmental changes in the loess of central China. Quat. Sci. Rev. 5, 489–495.
Liu, X., Hesse, P., Rolph, T., Begét, J., 1999. Properties of magnetic mineralogy of Alaskan loess: evidence for pedogenesis. Quat. Int. 62, 93–102. http://dx.doi.org/10.1016/S1040-6182(99)00027-0.
Liu, X.M., Hesse, P., Beget, J., Rolph, T., 2001. Pedogenic destruction of ferrimagnetics in Alaskan loess deposits. Aust. J. Soil Res. 39, 99. http://dx.doi.org/10.1071/SR99081.
Lund, S., Stoner, J., Channell, J., Acton, G., 2006. A summary of Brunhes paleomagnetic field variability recorded in Ocean Drilling Program cores. Phys. Earth Planet. Inter. 156, 194–204.
Matmon, A., Briner, J.P., Carver, G., Bierman, P., Finkel, R.C., 2010. Moraine chronosequence of the Donnelly Dome region, Alaska. Quat. Res. 74, 63–72. http://dx.doi.org/10.1016/j.yqres.2010.04.007.
McDowell, P.F., Edwards, M.E., 2001. Evidence of Quaternary climatic variations in a sequence of loess and related deposits at Birch Creek, Alaska: implications for the stage 5 climatic chronology. Quat. Sci. Rev. 20, 63–76.
Mock, C.J., Bartlein, P.J., Anderson, P.M., 1998. Atmospheric circulation patterns and spatial climatic variations in Beringia. Int. J. Climatol. 18, 1085–1104.
Muhs, D.R., Bettis, E.A., 2003. Quaternary loess-paleosol sequences as examples of climate-driven sedimentary extremes. Geol. Soc. Am. Spec. Pap. 370, 53–74.
Muhs, D., Budahn, J., 2006. Geochemical evidence for the origin of late Quaternary loess in central Alaska. Can. J. Earth Sci. 43, 323–337.
Muhs, D.R., Ager, T.A., Beann, J.M., Rosenbaum, J.G., Reynolds, R.L., 1998. An evaluation of methods for identifying and interpreting buried soils in late Quaternary loess in Alaska. U.S. Geol. Surv. Prof. Pap. 1615, 127–146.
Muhs, D.R., Ager, T.A., Beget, J.E., 2001. Vegetation and paleoclimate of the last

interglacial period, central Alaska. Quat. Sci. Rev. 20, 41–61.
Muhs, D.R., Ager, T.A., Bettis III, E.A., McGeehin, J., Been, J.M., Beget, J.E., Pavich, M.J., Stafford Jr., T.W., Stevens, D.A.S.P., 2003. Stratigraphy and palaeoclimatic significance of late Quaternary loess-palaeosol sequences of the Last Interglacial–Glacial cycle in central Alaska. Quat. Sci. Rev. 22, 1947–1986. http://dx.doi.org/10.1016/S0277-3791(03)00167-7.
Muhs, D.R., McGeehin, J.P., Beann, J., Fisher, E., 2004. Holocene loess deposition and soil formation as competing processes, Matanuska Valley, southern Alaska. Quat. Res. 61, 265–276. http://dx.doi.org/10.1016/j.yqres.2004.02.003.
Muhs, D.R., Ager, T.A., Skipp, G., Beann, J., Budahn, J., McGeehin, J.P., 2008. Paleoclimatic significance of chemical weathering in loess-derived paleosols of subarctic central Alaska. Arct. Antarct. Alp. Res. 40, 396–411.
Oches, E.A., Banerjee, S.K., Solheid, P.A., Frechen, M., 1998. High- resolution proxies of climate variability in the Alaskan loess record. In: Busacca, A.J. (Ed.), Dust Aerosols, Loess Soils and Global Change. Washington State University College of Agriculture and Home Economics, Miscellaneous Publication No. MISC0190, Pullman, pp. 167–170.
Péwé, T.L., 1955. Origin of the upland silt near Fairbanks, Alaska. Geol. Soc. Am. Bull. 66, 699–724. http://dx.doi.org/10.1130/0016-7606(1955)66[699:OOTUSN]2.0.CO;2.
Péwé, T.L., 1975a. Quaternary geology of Alaska. U.S. U.S. Geol. Surv. Prof. Pap. 835, 145.
Péwé, T.L., 1975b. Quaternary stratigraphic nomenclature in central Alaska. U.S. Geol. Surv. Prof. Pap. 862, 32.
Péwé, T.L., Wahrhaftig, C., Weber, F.R., 1966. Geologic Map of the Fairbanks Quadrangle, Alaska. U.S. Geol. Surv. Miscellaneous Investigations Map I-455, Scale 1: 250,000.
Péwé, T.L., Berger, G.W., Westgate, J.A., Brown, P.M., Leavitt, S.W., 1997. Eva interglaciation forest bed, unglaciated East-Central Alaska: global warming 125,000 years ago. Geol. Soc. Am. Spec. Pap. 319, 1–55.
Péwé, T.L., Westgate, J.A., Preece, S.J., Brown, P.M., Leavitt, S.W., 2009. Late Pliocene Dawson cut Forest bed and new tephrochronological findings in the gold Hill loess, east-central Alaska. Geol. Soc. Am. Bull. 121, 294–320. http://dx.doi.org/10.1130/B26323.1.
Preece, S.J., Westgate, J.A., Stemper, B.A., Pewe, T.L., 1999. Tephrochronology of late Cenozoic loess at Fair- banks, central Alaska. Geol. Soc. Am. Bull. 111, 71–90. http://dx.doi.org/10.1130/0016-7606(1999)111<0071:TOLCLA>2.3.CO;2.
Preece, S., Westgate, J., Alloway, B., Milner, M., 2000. Characterization, identity, distribution, and source of late Cenozoic tephra beds in the Klondike district of the Yukon, Canada. Can. J. Earth Sci. 37, 983–996.
Preece, S.J., Pearce, N.J.G., Westgate, J.A., Froese, D.G., Jensen, B.J.L., Perkins, W.T., 2011a. Old Crow tephra across eastern Beringia: a single cataclysmic eruption at the close of Marine Isotope stage 6. Quat. Sci. Rev. 30, 2069–2090. http://dx.doi.org/10.1016/j.quascirev.2010.04.020.
Preece, S.J., Westgate, J.A., Froese, D.G., Pearce, N.J.G., Perkins, W.T., 2011b. A catalogue of late Cenozoic tephra beds in the Klondike goldfields and adjacent areas, Yukon Territory. Can. J. Earth Sci. 48, 1386–1418.
Reger, R.D., Pinney, D.S., Burk, R.M., Wiltse, M.A., 1996. Catalog and Initial Analyses of Geologic Data Related to Middle to Late Quaternary Deposits, Cook Inlet Region, Alaska: State of Alaska Division of Geological and Geophysical Surveys Report of Investigation 95–96, p. 175. Fairbanks, AK.
Reyes, A.V., Froese, D.G., Jensen, B.J.L., 2010a. Permafrost response to last interglacial warming: field evidence from non-glaciated Yukon and Alaska. Quat. Sci. Rev. 29, 3256–3274. http://dx.doi.org/10.1016/j.quascirev.2010.07.013.
Reyes, A.V., Jensen, B.J.L., Zazula, G.D., Ager, T.A., Kuzmina, S., La Farge, C., Froese, D.G., 2010b. A late-Middle Pleistocene (Marine Isotope stage 6) vegetated surface buried by Old Crow tephra at the Palisades, interior Alaska. Quat. Sci. Rev. 29, 801–811. http://dx.doi.org/10.1016/j.quascirev.2009.12.003.
Roberts, H.M., 2012. Radiation measurements. Radiat. Meas. 47, 716–724. http://dx.doi.org/10.1016/j.radmeas.2012.03.022.
Russell, I.C., 1890. Notes on the surface geology of Alaska. Geol. Soc. Am. Bull. 1, 99–162.
Sanborn, P.T., Smith, C.A.S., Froese, D.G., Zazula, G.D., Westgate, J.A., 2006. Full-glacial paleosols in perennially frozen loess sequences, Klondike goldfields, Yukon Territory, Canada. Quat. Res. 66, 147–157. http://dx.doi.org/10.1016/j.yqres.2006.02.008.
Singer, B.S., Hoffman, K.A., 2005. Calibration of a pleistocene geomagnetic instability time scale (GITS) using 40Ar/39Ar-dated lavas. In: Am. Geophys. Union, Fall Meeting, Abstract #U42A-02, San Francisco.
Singer, B.S., Guillou, H., Jicha, B.R., Laj, C., Kissel, C., Beard, B.L., Johnson, C.M., 2009. $^{40}Ar/^{39}Ar$, K–Ar and $^{230}Th–^{238}U$ dating of the Laschamp excursion: a radioisotopic tie-point for ice core and climate chronologies. Earth Planet. Sci. Lett. 286, 80–88. http://dx.doi.org/10.1016/j.epsl.2009.06.030.
Singer, B.S., 2014. A Quaternary geomagnetic instability time scale. Quat. Geochronol. 21, 29–52. http://dx.doi.org/10.1016/j.quageo.2013.10.003.
Schweger, C.E., 2003. Paleoecology of two marine oxygen isotope stage 7 sites correlated by the Sheep Creek tephra, northwestern North America. Quat. Res. 60, 44–49. http://dx.doi.org/10.1016/S0033-5894(03)00089-9.
Schweger, C.E., Matthews, J.V., 1985. Early and Middle Wisconsinan environments of eastern Beringia: stratigraphic and paleoecological implications of the Old Crow tephra. Géogr. Physique Quaternaire 39, 275–290.
Seidenkrantz, M.S., Bornmalm, L., Johnsen, S.J., Knudsen, K.L., Kuijpers, A., Lauritzen, S.E., Leroy, S.A.G., Mergeal, I., Schweger, C., 1996. Two-step deglaciation at the oxygen isotope stage 6/5e transition: the Zeifen–Kattegat climate oscillation. Quat. Sci. Rev. 15, 63–75.
Spurr, J.E., Goodrich, H.B., 1898. Geology of the Yukon Gold District, Alaska: U.S., vol. 18. Geol. Surv. Annual Rep., pp. 87–392
Taber, S., 1943. Perennially frozen ground in Alaska: its origin and history. Geol. Soc. Am. Bull. 54, 1433–1548. http://dx.doi.org/10.1130/GSAB-54-1433.
Taber, S., 1953. Origin of Alaska silts. Am. J. Sci. 251, 321–336. http://dx.doi.org/10.2475/ajs.251.5.321.
Thorson, R.M., Bender, G., 1985. Eolian deflation by ancient katabatic winds: a late Quaternary example from the north Alaska Range. Geol. Soc. Am. Bull. 96, 702–709.
Thouveny, N., Creer, K.M., Blunk, I., 1990. Extension of the Lac du Bouchet palaeomagnetic record over the last 120,000 years. Earth Planet. Sci. Lett. 97, 140–161.
Thouveny, N., Carcaillet, J., Moreno, E., Leduc, G., Nérini, D., 2004. Geomagnetic moment variation and paleomagnetic excursions since 400 kyr BP: a stacked record from sedimentary sequences of the Portuguese margin. Earth Planet. Sci. Lett. 219, 377–396.
Thouveny, N., Bourlès, D., Saracco, G., Carcaillet, J., Bassinot, F., 2008. Paleoclimatic context of geomagnetic dipole lows and excursions in the Brunhes, clue for an orbital influence on the geodynamo? Earth Planet. Sci. Lett. 275, 269–284.
Turner, D., Ward, B.C., Bond, J.D., Jensen, B.J.L., Froese, D.G., Telka, A.M., Zazula, G.D., Bigelow, N.H., 2013. Middle to Late Pleistocene ice extents, tephrochronology and paleoenvironments of the White River area, southwest Yukon. Quat. Sci. Rev. 75, 59–77. http://dx.doi.org/10.1016/j.quascirev.2013.05.011.
Vlag, P., Oches, E., Banerjee, S., Solheid, P., 1999. The paleoenvironmental-magnetic record of the Gold Hill Steps loess section in central Alaska. Phys. Chem. Earth Part A 24, 779–783.
Weber, F., Hamilton, T., Hopkins, D., Repenning, C., Haas, H., 1981. Canyon Creek: a late Pleistocene vertebrate locality in interior Alaska. Quat. Res. 16, 167–180.
Westgate, J.A., Hamiltion, T.D., Gorton, M.P., 1983. Old Crow tephra: a new late Pleistocene stratigraphic marker across north-central Alaska and western Yukon Territory. Quat. Res. 19, 38–54.
Westgate, J., Walter, R., Pearce, G., Gorton, M., 1985. Distribution, stratigraphy, petrochemistry, and palaeomagnetism of the late Pleistocene Old Crow tephra in Alaska and the Yukon. Can. J. Earth Sci. 22, 893–906.
Westgate, J.A., Stemper, A.S., Péwé, T.L., 1990. A 3-my record of Pliocene-Pleistocene loess in interior Alaska. Geology 18, 858–861.
Westgate, J., Preece, S., Kotler, E., Hall, S., 2000. Dawson tephra: a prominent stratigraphic marker of Late Wisconsinan age in west-central Yukon, Canada. Can. J. Earth Sci. 37, 621–627.
Westgate, J., Preece, S., Froese, D., Pearce, N., Roberts, R., Demuro, M., Hart, W., Perkins, W., 2008. Changing ideas on the identity and stratigraphic significance of the Sheep Creek tephra beds in Alaska and the Yukon Territory, northwestern North America. Quat. Int. 178, 183–209. http://dx.doi.org/10.1016/j.quaint.2007.03.009.
Zazula, G.D., Froese, D.G., Westgate, J.A., La Farge, C., Mathewes, R.W., 2005. Paleoecology of Beringian "packrat" middens from central Yukon Territory, Canada. Quat. Res. 6, 189–198. http://dx.doi.org/10.1016/j.yqres.2004.11.003.
Zazula, G.D., Froese, D.G., Elias, S.A., Kuzmina, S., Mathewes, R.W., 2007. Arctic ground squirrels of the mammoth-steppe: paleoecology of late Pleistocene middens (24,000–29,450 ^{14}C yr BP), Yukon Territory, Canada. Quat. Sci. Rev. 26, 979–1003. http://dx.doi.org/10.1016/j.quascirev.2006.12.006.
Zazula, G.D., Froese, D.G., Elias, S.A., Kuzmina, S., Mathewes, R.W., 2011. Early Wisconsinan (MIS 4) Arctic ground squirrel middens and a squirrel-eye-view of the mammoth-steppe. Quat. Sci. Rev. 26 (30), 2220–2237.